



## EUROPEAN SOUTHERN OBSERVATORY

Organisation Européenne pour des Recherches Astronomiques dans l'Hémisphère Austral  
Europäische Organisation für astronomische Forschung in der südlichen Hemisphäre

ESO - European Southern Observatory  
Karl-Schwarzschild Str. 2, D-85748 Garching bei München

---

# Very Large Telescope Paranal Science Operations OmegaCAM User Manual

Doc. No. VST-MAN-OCM-23110-3110

Issue 108.1, Date 11/02/2021

J. Smoker, OmegaCAM consortium

Prepared .....

Date

Signature

A. Kaufer

Approved .....

Date

Signature

S. Mieske

Released .....

Date

Signature

This page was intentionally left blank

Document Change Record			
Issue	Date	Sect. / Paragr. affected	Reasons / Remarks
1.0	31.03.2004	all	first issue (PAE)
1.1	13.05.2004	most	changes in response to first RIXes (DBA, RHA)
2.0 draft	20.12.2006		small textual changes
		Appendix	Laboratory measurements of filter throughput
2.5	26.06.2011		update based on commissioning
2.6	11.08.2011	2.3	updates on filter naming and characteristics
2.7	05.09.2011	many, note 3.2.2 and 3.4.4	Update by ESO-PSO after science verification
2.7.1.	14.09.2011		Minor language updates by ESO-USD
3.0.	20.12.2011	most	Update based on commissioning reports and start of survey operations
			Manual officially taken over by ESO
90.0	27.02.2012	Sects. 3.4.1 & 3.7.1	Update to overheads and PSF
			Version number aligned with Period number
90.1	24.05.2012	Sects. 3.4.4	Update to overheads: IAStar and telescope offset
91.0	15.12.2012	Sect. 3.7.5.	New Section 3.7.5. about vignetting by wind mast
92.0	07.03.2013	Sect. 3.4.4.	Update to overheads: parallelised readout
92.0	07.03.2016		and preset/filter-setup
92.1	23.05.2013	Sect. 3.4.4.	Update to overheads: first offset in a template is 5s shorter
95.0	23.08.2014	Sect. 2.9.1.	Performances of the new Baffling system installed in P94
98.0	04.07.2016	All	ADC to be removed from templates in P99.
98.0	04.07.2016	All	Note on short exposure times added.
98.0	04.07.2016	Sect. 4.1	Occasional jumps in bias levels under investigation.
98.0	04.07.2016	Table 1	Mismatch between gain in manual and FITS headers under investigation.
98.0	04.07.2016		
99.0	12.09.2016		No changes.
99.1	23.12.2016	Sect 2.4	Comment on the minimum integration time
99.1	23.12.2016	Sect 2.10	Comment on tests of the laser guide star facility
100.2	02.07.2017	Sect 2.4	Comment on the minimum integration time. Figure added.
101.1	30.08.2017	Sect 3.1	Change in type of OCam proposals accepted by ESO. See the call for proposals.
101.2	22.11.2017	Sect 3.7	Figure added showing fraction of OBs with ellipticity more than 20 percent against elevation.
101.2	22.11.2017	Sect 2.10	Images showing 4GLSF laser in r_SDSS band.
101.3	22.11.2017	All	References to p2 added.
102.1	26.02.2018	Sect. 3.7	Comment that from P101 zenith distances of less than 7 degrees will normally be avoided in service mode.
102.2	18.02.2018	Sect. 3.4.2	No return to origin if last template in the OB for OMEGACAM_img_obs_jitter
103.0	30.08.2018		References to p2pp removed and replaced by p2
104.1	20.02.2019		No changes
105.1	28.02.2019		Proposal preparation now in p1 instead of ESOFORM. ETC turbulence category and water vapour introduced.
105.2	24.11.2019	Sect. 2.10	Effect of laser on OmegaCAM observations shown.
		Sect. 3.3	Observing constraints section slightly modified.
		Sect. 4.2	Data reduction of PI programmes with CASU.
106.2	11.05.2020		No changes
107.2	11.11.2020		No changes
107.3	09.12.2020	Sect 4.1.1	Method to calibrate HAlpha and NB659 added.
108.1	12.02.2021	Sect 1.1	CCD 77 currently not working.

## Contents

<b>1</b>	<b>Introduction</b>	<b>1</b>
1.1	CCD 77 . . . . .	1
1.2	Credits . . . . .	1
1.3	Scope . . . . .	1
1.4	More Info . . . . .	1
1.5	References . . . . .	1
1.6	Acronyms . . . . .	2
<b>2</b>	<b>Instrument characteristics</b>	<b>4</b>
2.1	Overview . . . . .	4
2.2	Detector Mosaic . . . . .	8
2.2.1	The 268-Million Pixel Science Array . . . . .	8
2.2.2	Auxiliary CCDs . . . . .	14
2.3	Filters . . . . .	14
2.3.1	Note on filter magazines . . . . .	16
2.3.2	Providing Private Filters . . . . .	18
2.4	Shutter . . . . .	19
2.5	Auto-Guiding and Focussing . . . . .	20
2.5.1	VST Guide Probe . . . . .	21
2.5.2	Auto-guiding with OmegaCAM . . . . .	21
2.5.3	Differential Guiding . . . . .	21
2.5.4	Image Analysis with OmegaCAM . . . . .	21
2.5.5	Traffic rules between science and auxiliary CCD readouts . . . . .	22
2.6	Calibration lamps . . . . .	22
2.7	Photometric Properties . . . . .	22
2.8	Astrometric Properties . . . . .	22
2.9	Flat fielding of OmegaCAM data / Illumination correction . . . . .	23
2.9.1	Performances of the new Baffling system . . . . .	23
2.10	Effect of the laser guide star facility on OmegaCam . . . . .	27
<b>3</b>	<b>Observing with OmegaCAM</b>	<b>31</b>
3.1	Offsetting Modes and Observing Strategies . . . . .	31



---

3.1.1	Offsetting Modes . . . . .	31
3.1.2	Observing Strategies . . . . .	32
3.2	Atmospheric Refraction and Dispersion . . . . .	32
3.2.1	Atmospheric Refraction . . . . .	32
3.2.2	Atmospheric Dispersion . . . . .	33
3.3	OB preparation . . . . .	34
3.3.1	Target acquisition . . . . .	34
3.3.2	Scientific exposure . . . . .	35
3.3.3	Dither and jitter patterns . . . . .	35
3.4	The Observing templates . . . . .	35
3.4.1	Target Acquisition Templates . . . . .	35
3.4.2	Science Templates . . . . .	35
3.4.3	Nighttime Calibration . . . . .	36
3.4.4	Overheads . . . . .	36
3.5	Survey Area Definition Tool . . . . .	38
3.6	Selecting exposure times and number of sub-exposures . . . . .	38
3.7	Special features of the data . . . . .	38
3.7.1	Point Spread Function . . . . .	38
3.7.2	CCD blemishes and particle hits . . . . .	40
3.7.3	Ghosts and reflections . . . . .	40
3.7.4	Sky concentration . . . . .	41
3.7.5	Vignetting close to wind mast position . . . . .	41
3.7.6	Diffraction Spikes . . . . .	44
3.7.7	Fringes . . . . .	44
3.7.8	Remanence . . . . .	44
3.7.9	CCD Crosstalk . . . . .	45
<b>4</b>	<b>Calibrating and Reducing OmegaCAM data</b>	<b>47</b>
4.1	Calibration Plan . . . . .	47
4.1.1	Calibration of HALPHA and NB659 data . . . . .	48
4.2	Data reduction Pipeline . . . . .	49
4.3	Quality Control . . . . .	50
<b>A</b>	<b>Filter throughput curves</b>	<b>51</b>

A.1	Broad band Sloan filters ( $u'g'r'i'z'$ ) . . . . .	51
A.2	Segmented Broad-band filters (Johnson B and V) . . . . .	57
A.3	Narrow-band filters (Strömgren $v$ and $H\alpha$ ) . . . . .	57
A.4	Radial variations in bandpass . . . . .	58
<b>B</b>	<b>Detector response curves</b>	<b>59</b>

## List of Tables

1	Basic CCD characteristics . . . . .	10
2	Properties of all 32 CCDs . . . . .	14
3	Filters available in OmegaCAM . . . . .	17
4	Current OmegaCAM filter distribution. The opaque filter is required to protect the instrument when it is not in operation. . . . .	18
5	Magnitude zero points for the SDSS filter set. . . . .	23
6	Illumination correction functions . . . . .	23
7	Key difference between the dither and jitter modes. . . . .	32
8	Maximum airmasses without using the ADC . . . . .	34
9	Overhead times for observations . . . . .	37
10	OmegaCAM Photometric Standard Star Fields . . . . .	49

## List of Figures

1	Schematic drawing of OmegaCAM . . . . .	4
2	Optical layout of the VST . . . . .	5
3	Layout of the CCDs in the focal plane . . . . .	6
4	Spot Diagrams . . . . .	7
5	Photograph of the detector mosaic . . . . .	9
6	Single CCD pixel layout . . . . .	11
7	Schematic of CCD readout . . . . .	12
8	Linearity of the CCDs . . . . .	13
9	Filter times CCD throughput . . . . .	15
10	An OmegaCAM filter . . . . .	16
11	Shadow cast by the cross in composite filters . . . . .	17
12	Orientation of filter as function of magazine . . . . .	18

13	The shutter unit . . . . .	19
14	Counts vs exposure time . . . . .	20
15	Illumination correction derivation for OmegaCAM Sloan r . . . . .	24
16	Asymmetric straylight in flatfields for OmegaCAM Sloan r . . . . .	25
17	Raw dome flat divided by raw twilight flat for OmegaCAM Sloan r . . . . .	26
18	. . . . .	27
19	. . . . .	28
20	. . . . .	29
21	. . . . .	30
22	. . . . .	30
23	Limit on exposure time due to atmospheric refraction . . . . .	33
24	OmegaCAM PSF anisotropies . . . . .	39
25	OmegaCAM IQ distribution, collected between August and December 2011 . . . . .	39
26	. . . . .	40
27	Example ghost reflection . . . . .	42
28	Reflection from a star outside the field . . . . .	43
29	Vignetting by wind mast . . . . .	43
30	Fringe maps in $i'$ and $z'$ band . . . . .	44
31	Crosstalk between CCDs 93–96 . . . . .	46
32	Frequency of calibration observations . . . . .	48
33	Filter measurement location and coordinate system . . . . .	51
34	$u'$ filter throughput . . . . .	52
35	$g'$ filter throughput . . . . .	53
36	$r'$ filter throughput . . . . .	54
37	$i'$ filter throughput . . . . .	55
38	$z'$ filter throughput . . . . .	56
39	CCD Quantum efficiency curves . . . . .	59

## 1 Introduction

### 1.1 CCD 77

From 2020-Mar-24 to 2020-Nov-15 OmegaCAM was out of operations. When observations were resumed, CCD-77 was found not to be operational which at the time of updating this manual (12-Feb-2021) is still the case. Attempts are ongoing to fix this problem. Please see the OmegaCAM news page for the latest information.

### 1.2 Credits

This manual is largely based on the OmegaCAM user manual drafted and maintained by the OmegaCAM consortium (Konrad Kuijken, Bernard Muschielok, Andrea Baruffolo) between 2004 and 2011 until end of OmegaCAM commissioning. It also includes content from the OmegaCAM DFS Commissioning Reports, and input from the OmegaCAM IOT. It will be updated continuously by Paranal Science Operations, as survey operations evolve and more experience is gathered.

### 1.3 Scope

OmegaCAM is the wide-field imager for the Cassegrain focus of the VLT Survey Telescope (VST) on Paranal, a 2.6m modified Ritchie-Chretien alt-az telescope designed specifically for wide-field imaging. It is the only instrument on this telescope, and is operated most nights. In principle all observations are carried out in service mode. Its main function is to perform large optical imaging surveys, which may be used to feed the VLT telescopes with targets. With its wide field, broad-band filter set, and image quality matched to Paranal seeing conditions, OmegaCAM is well-suited to this task.

This document serves as a user manual for those planning or preparing observations with OmegaCAM. It describes the main instrument characteristics, and how to observe with it using Observation Blocks and Observing Templates.

The manual has been previously edited by F. Selman, G. Beccari, S. Mieske and G. Carraro.

The most recent version of this manual is kept at

<http://www.eso.org/sci/facilities/paranal/instruments/omegacam/doc/>.

### 1.4 More Info

Further information can be obtained by contacting [usd-help@eso.org](mailto:usd-help@eso.org) and consulting the public OmegaCAM webpage <http://www.eso.org/sci/facilities/paranal/instruments/omegacam/>. ESO Quality Control Pages are found at <http://www.eso.org/observing/dfo/quality/ALL>

### 1.5 References

[RD1] Template Manual, VST-MAN-OCM-23100-3111,  
see <http://www.eso.org/sci/facilities/paranal/instruments/omegacam/doc/>.

[RD2] Calibration Plan, VST-PLA-OCM-23100-3090,  
see <http://www.eso.org/sci/facilities/paranal/instruments/omegacam/doc/>.

[RD3] DFS User Requirements, VST-SPE-OCM-23100-3050,  
see <http://www.eso.org/sci/facilities/paranal/instruments/omegacam/doc/>.

[RD4] WFI documentation, see <http://www.ls.eso.org/lasilla/sciops/2p2/E2p2M/WFI/>.

[RD5] P2 instructions, see <https://www.eso.org/sci/observing/phase2/p2intro.html>.

[RD6] OmegaCAM public webpage, see <http://www.eso.org/sci/facilities/paranal/instruments/omegacam/>.

[RD7] ESO QC web page, see <http://www.eso.org/observing/dfo/quality/ALL/>

## 1.6 Acronyms

ADC: Atmospheric dispersion compensator, a device which corrects for the chromatic effects of the atmosphere at low elevations. Note that the ADC is not used in OmegaCam and will be removed from the templates in P99.

CCD: Charge-couple device, a solid-state, panoramic light detector of high quantum efficiency.

CTE: Charge Transfer Efficiency. The efficiency of the charge transport during readout.

DFS: Data Flow System.

DIMM: Differential Image Motion Monitor

e2v: Manufacturer of the OmegaCAM CCDs.

ETC: Exposure Time Calculator, a software tool provided by ESO as an aid in planning observations.

FOV: Field-of-view

FWHM: Full Width at Half-Maximum.

IQ: Image Quality

MPG: Max Planck Gesellschaft.

OB: Observation Block, a set of instructions to telescope and instrument to carry out a specific observation.

OmegaCAM: The wide-field CCD camera for the VST.

P1: Phase 1 Proposal Preparation. From P105 this will be done using a dedicated web interface and not using ESOFORM.

P2: Phase 2 Proposal Preparation, the process at ESO in which the users define the OBs for their approved programmes by means of special software. The new p2 is a web-based application, see: <https://www.eso.org/p2/>

PA: Position Angle, orientation of the field of view on the sky. For VST/OmegaCAM, PA=0 means that North is in positive y-direction and East is in negative x-direction.

PSF: Point-Spread-Function

RMS: Root-mean square.

SADT: Survey Area Definition Tool

SDSS: Sloan Digital Sky Survey, a large imaging and spectroscopy survey of (mostly) the Northern hemisphere. OmegaCAM's science filter set include the five SDSS filters  $u'g'r'i'z'$ .

USM: Universitätssternwarte München

USNO: US Naval Observatory. Their all-sky catalogue is used for astrometric calibration of Omega-

CAM data.

VLT: Very Large Telescope, four 8m telescopes on ESO's Paranal Observatory.

VST: VLT Survey Telescope, a 2.6m telescope at ESO's Paranal Observatory dedicated to optical surveys, and host to OmegaCAM.

WFI: Wide-Field Imager, an 8-CCD mosaic camera on the ESO/MPG 2.2 telescope on La Silla with similar pixel scale and sensitivity to OmegaCAM.

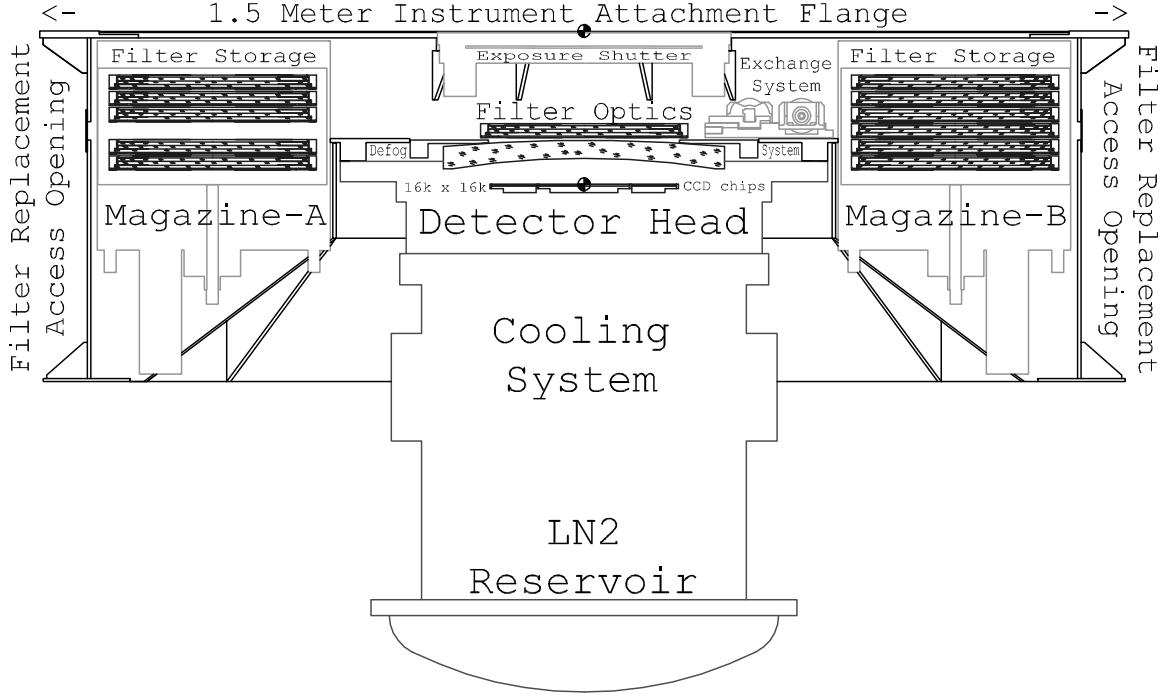


Figure 1: Schematic view of the instrument. Key components are labelled.

## 2 Instrument characteristics

### 2.1 Overview

OmegaCAM (see Fig. 1) is the wide-field imager for the Cassegrain focus of the VLT Survey Telescope (VST) on Paranal, a 2.6m modified Ritchie-Chretien alt-az telescope designed specifically for wide-field imaging. It is the only instrument on this telescope, and is operated most nights. In principle all observations are carried out in service mode.

The VST/OmegaCAM system is designed for good seeing-limited image quality over a wide field. The telescope has an actively controlled meniscus primary mirror, an active secondary, and an image analysis system. It contains two interchangeable correctors: one is a high-throughput two-lens corrector which works in  $u'-z'$  bands, the other contains an Atmospheric Dispersion Compensator (ADC) for work at lower elevations. The ADC has almost no throughput in the  $u'$  band. Note that from P99 the ADC will not be offered.

The optical layout of the VST is illustrated in Fig. 2.

The VST provides a 1 degree unvignetted field of view, which OmegaCAM samples with a 32-CCD, 16k x 16k detector mosaic (Fig. 3) at 0.21 arcsec per pixel (0.213 for the two-lens corrector, 0.215 for the ADC configuration). Each CCD is of 2k x 4k format and subtends  $\sim 7.3' \times 14.6'$  on the sky. The CCDs are thinned, blue-sensitive, 3-edge butttable CCD44-82 devices from e2v of high (but not perfect) cosmetic quality. Image quality is specified such that in the absence of seeing 80% of the energy from a point source should fall within a 2x2 pixel area over the full field (see example spot diagrams in Fig 4). The field distortion is very low, so that the image scale is virtually constant over the whole field. There are narrow gaps between the CCDs: the overall geometric filling factor of the array is 91.4%.

In addition to the 32 CCDs making up the science array, OmegaCAM also contains four auxiliary

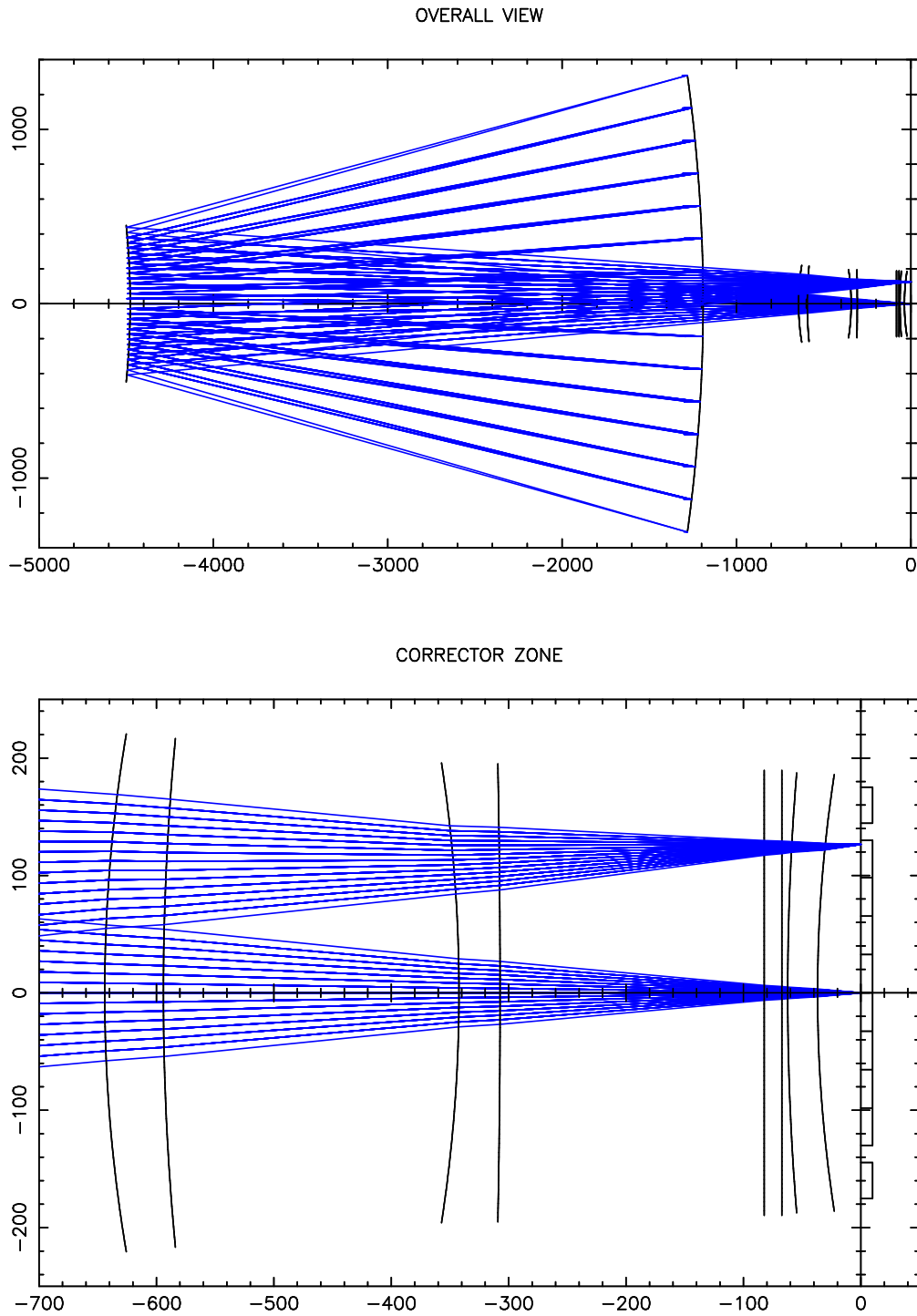


Figure 2: Optical layout and selected light paths through the VST. The configuration with the two-lens corrector is shown. The bottom panel shows a zoom onto the corrector optics: the incoming light passes through two spherical lenses, a planar filter, and the spherical dewar entrance window before reaching the CCDs on the right. Scales are in mm.



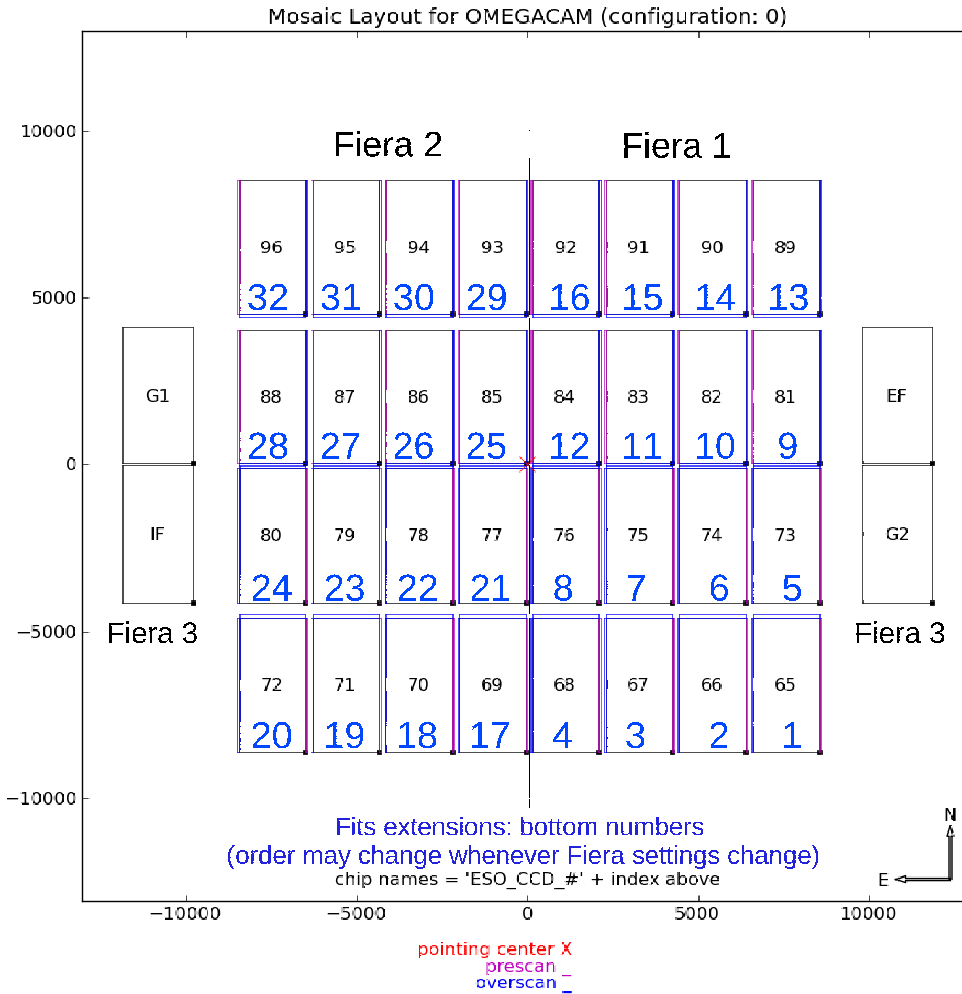


Figure 3: The layout of the 32 science CCDs and the four auxiliary CCDs in the focal plane. The science array covers a 1 degree x 1 degree area of sky, with 16k x 16k pixels of 0.21 arcsec. All CCDs fit inside a circle of diameter 1.4 degrees on the sky. (Note that this is the layout as seen from below, i.e., the projection of the array onto the sky.)

OmegaCAM data are delivered as multi-extension FITS files. The CCD name (#65–96) is included in the header of each fits extension. CCDs can also be identified by the number of their fits extension, but beware: this order may change from what is shown in the Figure whenever CCD controller parameters are changed.

Two of the auxiliary CCDs are mounted out of the focal plane (Extra- and Intra-focal; IF & EF), at displacements  $\pm 2$ mm, in order to enable image analysis and real-time active optics corrections. Auxiliary CCDs G1 and G2 are used for guiding. All 4 auxiliary CCDs are partly vignetted around their respective outermost corner.

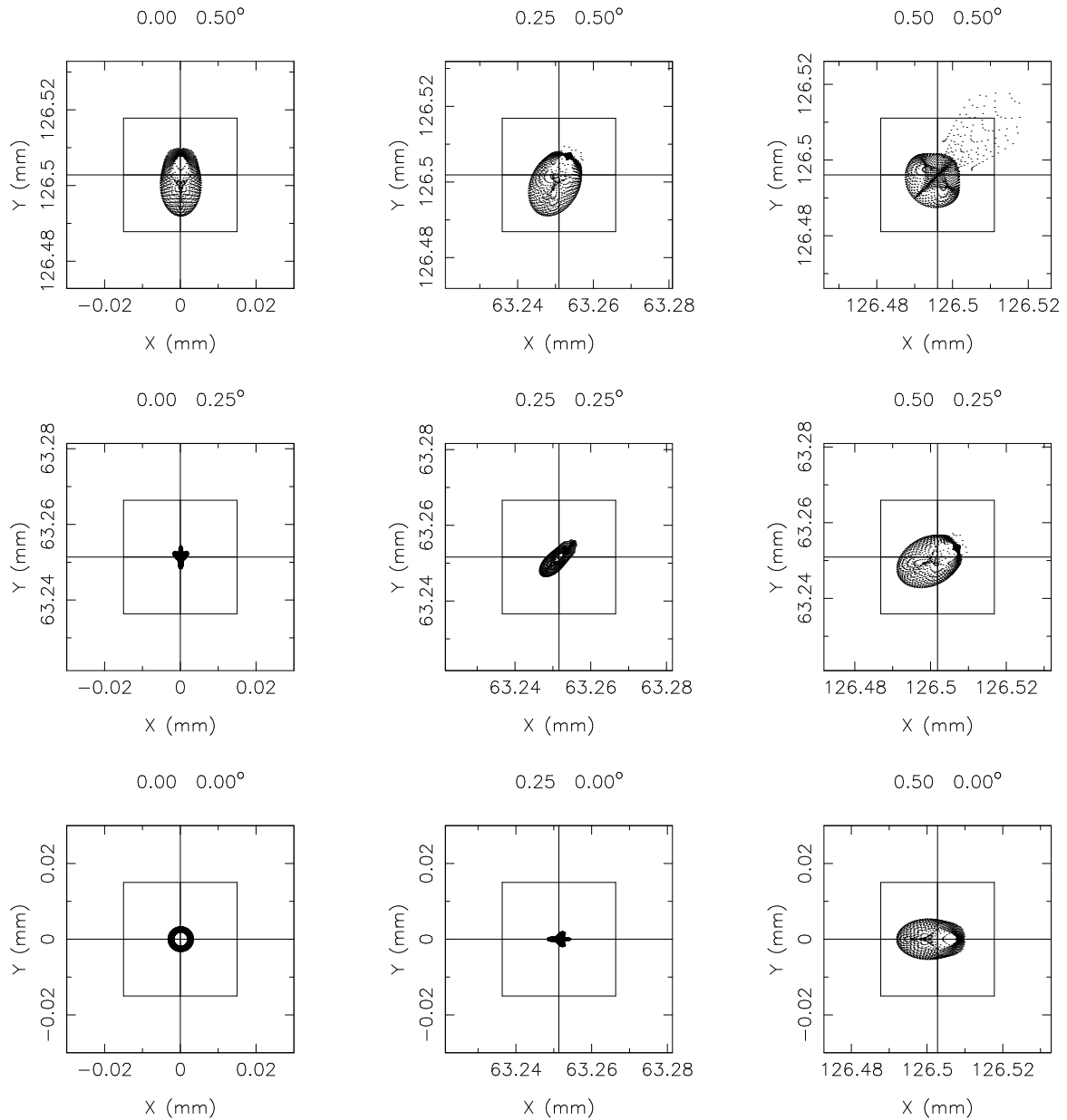


Figure 4: Sample spot diagrams for 500nm light in a quadrant of the OmegaCAM focal plane. A 2x2 pixel grid (30μm × 30μm, corresponding to 0.43'') is shown as well.

CCDs around the edges of the field. Two of these are used for autoguiding, so that both field position and rotation can be tracked accurately. The other two auxiliary CCDs are mounted 2mm outside the focal plane (one in front, one behind), and are used for recording defocused star images for on-line analysis of the image quality. The CCD layout in the focal plane is shown in Fig. 3. A photograph of the detector mosaic is shown in Fig. 5.

OmegaCAM contains a 12-slot filter exchange mechanism, subdivided into two cabinets of six slots each. Currently the available filters include the Sloan  $u'g'r'i'z'$  set, Johnson  $B$  and  $V$  filters, several narrow-band filter mosaics, a Strömgren  $v$  filter, and a special calibration filter (see Table 3).

OmegaCAM data are taken in the context of a calibration plan [RD2] that ensures that all data can be photometrically and astrometrically calibrated to 0.05 magnitudes and 0.1 arcsec rms precision, respectively. See Sect. 4.1.

Compared to the wide-field imager (WFI [RD4]) on the ESO/MPG La Silla 2.2m telescope, OmegaCAM on the VST offers

1. a four times larger field
2. better cosmetic quality CCDs
3. a primary mirror of 1.4 times the area
4. year-round operation in service mode
5. better image quality due to active telescope optics, astro-climate
6. the Sloan filter set (but only very few narrow-band filters)

## 2.2 Detector Mosaic

### 2.2.1 The 268-Million Pixel Science Array

The central 32 CCDs of OmegaCAM form the science array, the heart of the instrument. Basic characteristics of the CCDs are found in Table 1. Consult also the OmegaCAM QC webpages [RD7] for up-to-date information. The CCD type is e2v, CCD44-82.

The packaging of a single CCD is illustrated in Fig. 6. The light-sensitive area consists of 4100x2048 pixels, surrounded by a border whose width is 0.16mm on the short side opposite the readout register, 0.5mm along the long sides of the CCD, and 5mm on the side of the readout register. Unavoidably therefore, there are small 'dead zone' gaps in the science array between the light-sensitive areas of neighbouring CCDs. How the CCDs are mounted together in the array is indicated in Figs. 3 and 5. The CCDs are mounted as closely as possible. The resulting average gap sizes are:

- between the long sides of the CCDs: 1.5mm (100 pix=21.5")
- central gap along the short sides: 0.82mm (55 pix=11.8")
- wide gap along short sides: 5.64mm (376 pix=80.5")
- between science array and auxiliary CCDs: 15.9mm (1060 pix)

All CCDs are read out at 280kpix/s, through one amplifier port each (in all cases situated at the "left" end of the readout register). The resulting image comes with 48 columns of pre- and overscan, and 100 rows of vertical overscan. Because of their construction and the way they are arranged in the mosaic, all CCDs are read out along their long side, in a direction away from the center of the

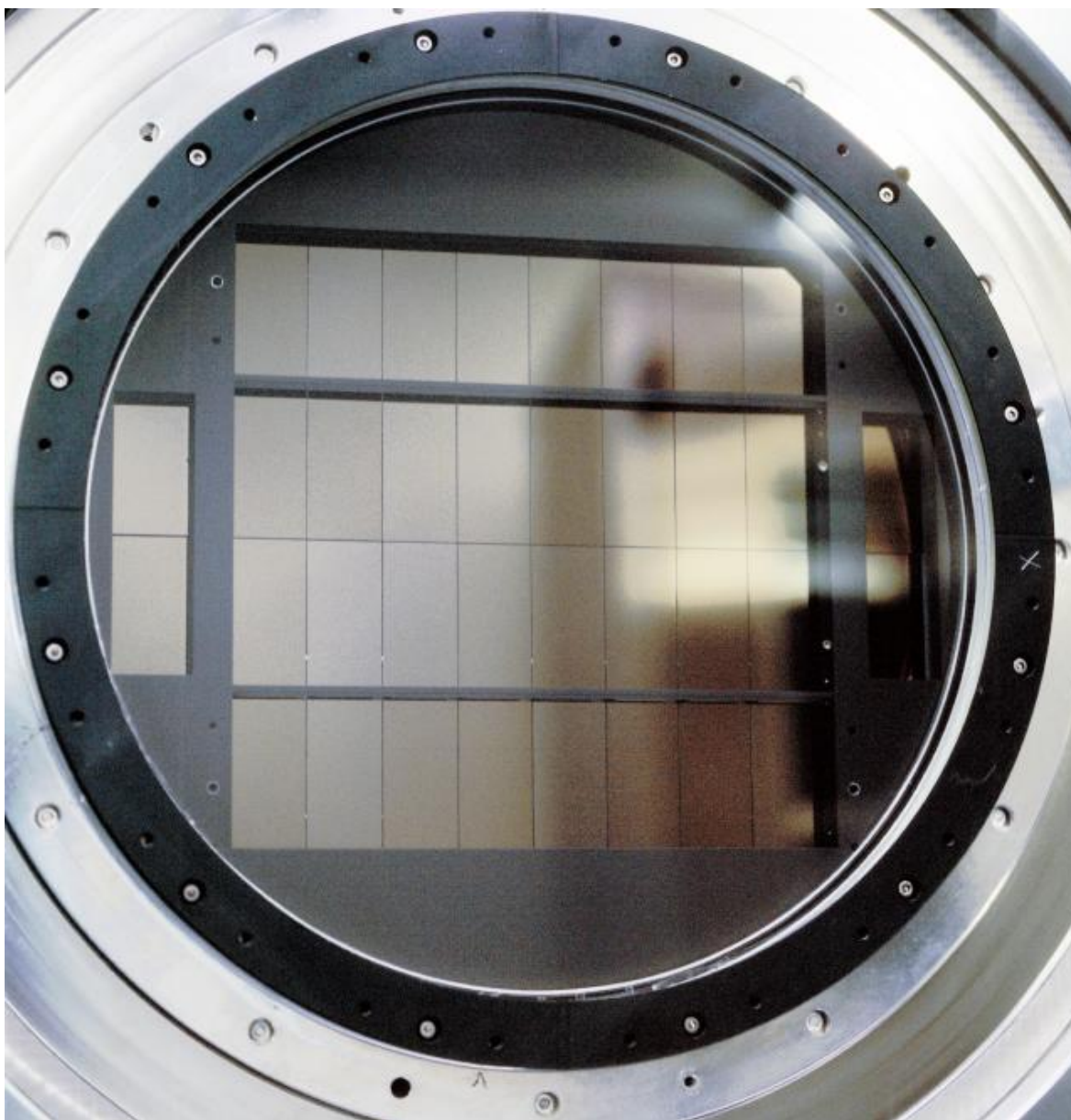


Figure 5: Picture of the 36 CCDs mounted behind the dewar window. Note the black strips that cover the gaps between the CCDs: they prevent reflection of light off the bright bond wires of each detector. Slight vignetting is observed near these strips, and on the long outer sides of the four corner CCDs.

CCD Parameter	Value
CCD type	Marconi / e2v / CCD 44 - 82 - 1 - A57 thin devices (20 $\mu$ m)
Pixel size	15 $\mu$ m
Format	Active Pixel Area 2048 x 4102 pixels (2048x4100 used) 50 horizontal pre- and 50 overscan pixels
Default Read Speed	280 kpix/sec
Flatness	< 20 $\mu$ m peak to valley
R.O.N. (not including system noise)	2 e- at 50 kpix/sec 4 e- at 500 kpix/sec 6 e- at 1000 kpix/sec
Full R.O.N. (including system noise) at default read speed	5-7 e-
Gain [e-/ADU]	$\sim$ 2.6 with 10% chip-to-chip RMS
Output Amplifiers	2 identical output amplifiers with integrated post chip amplifiers. Charge can in principle be read through either one completely or through both of them simultaneously. In practise, only the respective "left" one is used.
Device Layout	No frame transfer option, 3 phase parallel register (non split), 3 phase serial register (split)
Dump Drain	A dump drain exists parallel to the serial readout register, so that lines can be discarded as a whole
Cosmetics	A global defect budget exists, specifying the overall defects for all of the 40 science devices (Cosmetically the final device cosmetics are much better than devices used for the WFI)
CTE	> 0.999995 per parallel or serial shift
Horizontal Transfer Frequency	2 Mpixels/sec
Vertical Transfer Frequency	15-20 klines/sec
Full Well / Linearity	>200 000 e-. Serial full well is at least 2 times the pixel full well and the summing full well is at least 4 times the pixel full well. These full well values correspond to the maximum charge that can be handled while attaining the CTE specified. Amplifier full well is around 200 000 e-. Amplifier full well refers to the limit of linearity, i.e. the maximum amount of charge that can be amplified while producing output that matches a linear response to within 1 %.
Dark Current	< 2 e- / pixel / hour (at operating temperature of $-120^{\circ}\text{C}$ )
Cross talk	There is cross talk at the level of < 0.4% between CCDs 93-96.
Gain variations	CCDs # 87 and 88 shows day-to-day gain variations of 1-2% RMS.
Cosmic Ray Sensitivity	< 3 events / square cm and minute
Optical Coating	Single layer anti reflection coating astro BB (with thickness 42nm instead of 46nm)
Package design	Four side buttable (fourth side with larger gap), Invar package with integrated PT100 temperature sensor

Table 1: Basic characteristics of the OmegaCAM CCDs. See also Table 2 and Fig. 8. There is a mismatch between the value of gain in the headers and the manual which is currently under investigation.

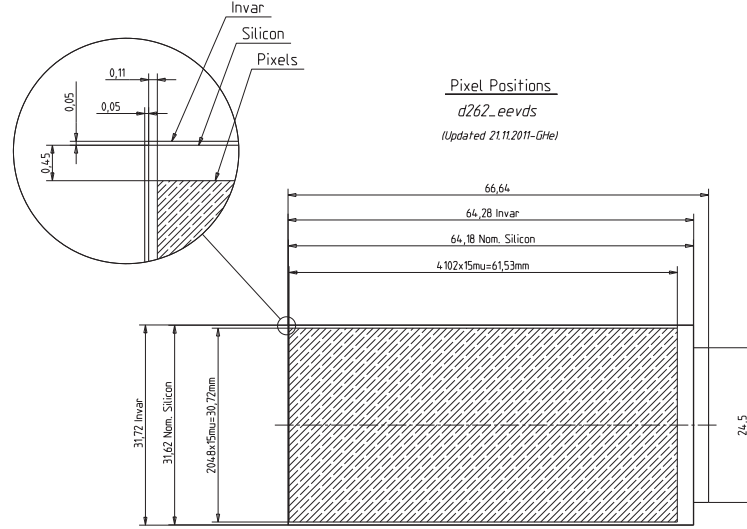


Figure 6: The light-sensitive area of a single CCD. Units are in mm, size of a single pixel is  $15 \mu$ .

mosaic. In the lower half of the CCD array, the readout register is at the "bottom" (southern edge) of the CCDs, whereas in the upper (northern) half the CCDs are rotated through 180 degrees.

The readout sequence is illustrated in Fig. 7. The science mosaic is read out by two FIERA systems, one for each half (East/West) of the array. Total readout time is 29sec. Combined with other overheads, principally the time needed to wipe the array before a new exposure, this leads to a total minimum shutter-closed time between successive exposures of 40 seconds.

Generally the CCDs in the array are similar, but they do differ in detail. A number of properties of the CCDs are tabulated in Table 2, in a format that corresponds to their layout in the science array (top view). At the default sky position angle of zero degrees this layout corresponds to N at the top, and East to the *right*.

Complete QE curves for each of the CCDs are given in Appendix B.

All CCDs but three have parallel and serial CTE above 0.999995, the exceptions being:

- CCD #65 and #96, which have serial CTE 0.999994
- CCD #72 which has serial CTE 0.999993

With a gain of ca. 2.6 electrons per ADU, the analog-to-digital conversion of the amplifier output of each CCD saturates before the CCD full-well capacity of over 200.000 electrons. Below this saturation the response of the CCDs is linear to within 1%, as can be seen from Fig. 8.

The flat fields of the CCDs show different behaviour, dependent on the wavelength. In the  $u'$  band, the flat fields show a diagonal, diamond-like pattern, which is caused by the thinning process. A few of the CCDs (#65, 66, 86, 87) also show an 'ink pattern', areas of very high UV sensitivity (the origin of this feature is unknown). At intermediate wavelengths ( $g'$ ,  $r'$ ) the flat fields are reasonably featureless. At longer wavelengths ( $i'$  and particularly  $z'$ ), fringing occurs, leading to swirling patterns reminiscent of a thin film of oil on water. All artifacts can be removed in data reduction.

The efficiency of the filters, folded with the detector response, is plotted in Fig. 9. Detailed analysis

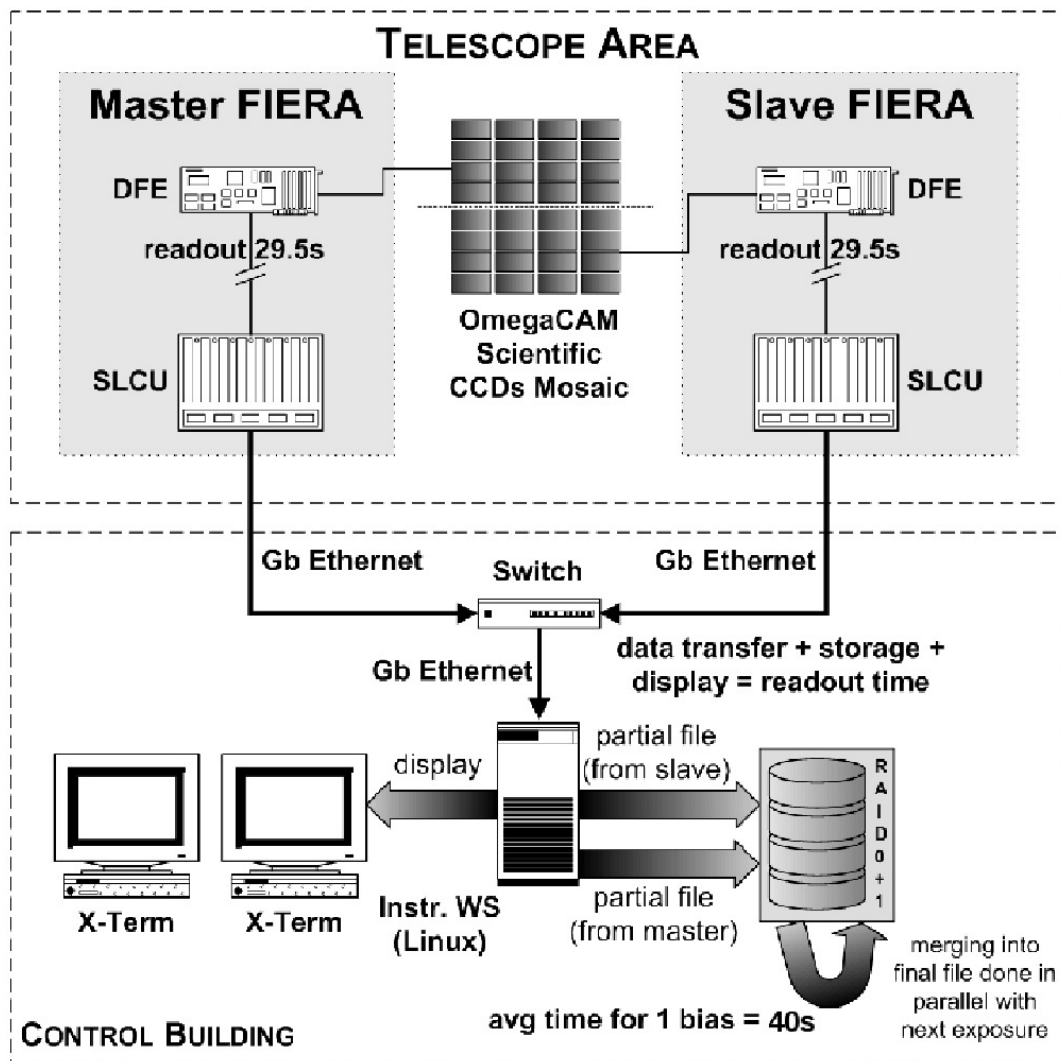


Figure 7: Data flow diagram for readout of the OmegaCAM science array.

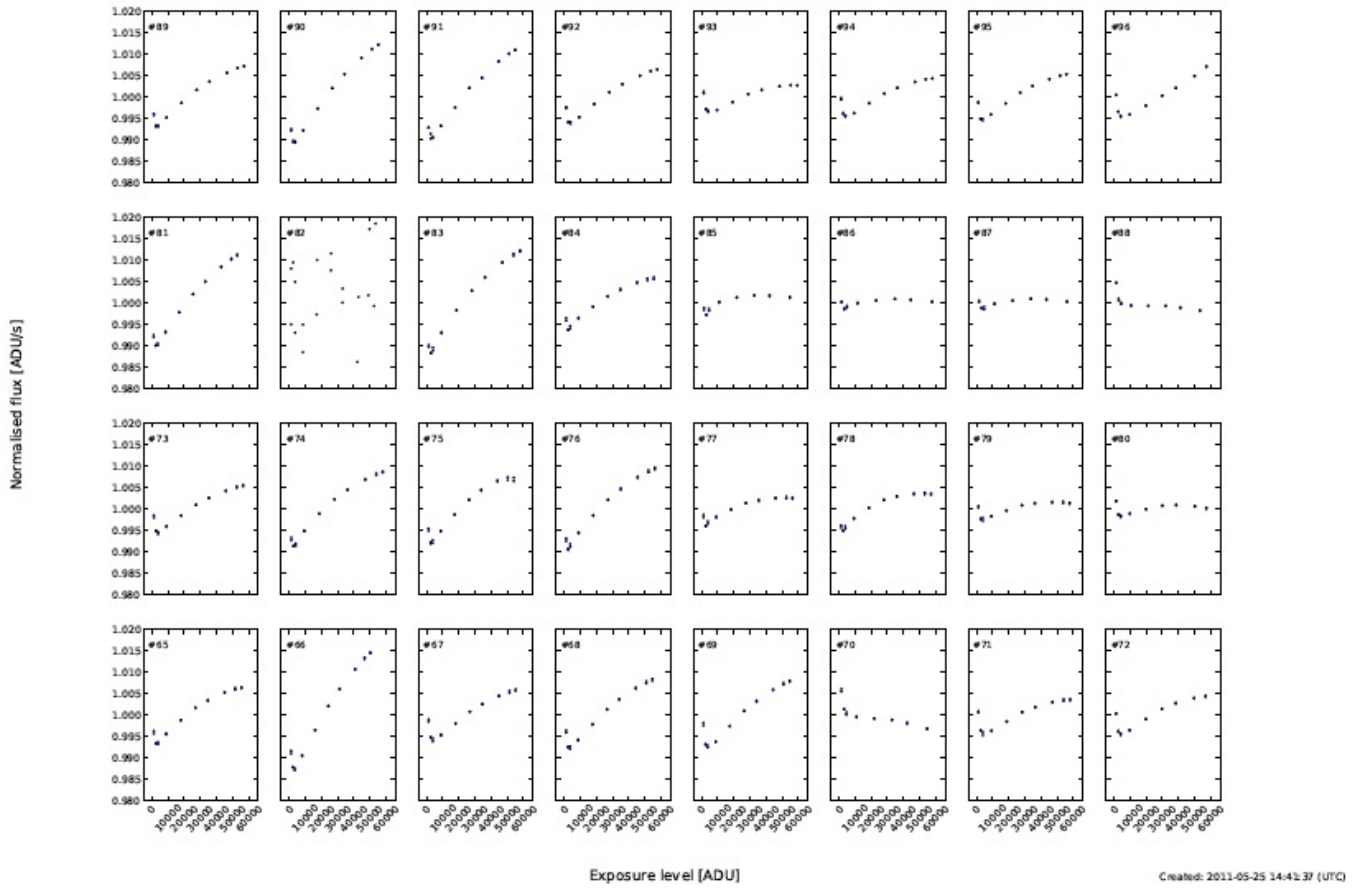


Figure 8: Plot of the linearity of the response of each CCD, as a function of illumination level. (Obtained by exposing the mosaic to a calibration lamp, with varying exposure times).



Table 2: Properties of all 32 CCDs

**N (at PA 0 degrees)**

<div style="border: 1px solid black; padding: 5px; width: fit-content;">           CCD number            gain (e-/ADU)            readnoise (e-)            # hot pixels            # cold pixels            dark current (ADU/hr)         </div>	#89	#90	#91	#92	#93	#94	#95	#96	<b>E</b>
	2.37	2.52	2.62	2.56	2.56	2.78	2.73	2.37	
	6.52	6.23	5.98	6.03	5.15	5.61	6.90	5.17	
	50	14	11	24	18	16	17	18	
	3143	16719	8891	4926	7037	15038	10134	7222	
	0.50	0.46	0.36	0.47	0.27	0.37	0.15	0.34	
	#81	#82	#83	#84	#85	#86	#87	#88	
	2.57	2.56	2.56	2.46	2.40	2.32	2.39	2.52	
	5.20	5.05	5.22	5.06	5.19	4.82	5.10	5.22	
	25	3490	28	825	11	13	19	9	
	8698	2816	9611	5713	9742	6420	8570	9553	
	0.36	0.28	0.41	0.31	0.33	0.40	0.37	0.38	
	#73	#74	#75	#76	#77	#78	#79	#80	
	2.40	2.48	2.52	2.44	2.66	2.71	2.67	2.57	
	4.70	5.18	5.12	4.97	5.95	5.31	5.36	5.17	
	7	16	18	20	13	7	58	50	
	3811	2692	2765	2802	2683	2660	2911	4329	
	0.35	0.22	0.21	0.28	0.33	0.26	0.24	0.29	
	#65	#66	#67	#68	#69	#70	#71	#72	
	2.39	2.59	2.49	2.55	2.48	2.23	2.54	2.39	
	4.73	5.10	5.20	5.42	5.28	4.69	5.08	4.83	
	7	131	25	109	18	20	16	13	
	2807	5363	2956	4163	3003	5783	7371	4191	
	0.30	0.36	0.26	0.30	0.25	0.31	0.27	0.28	

of the filter throughput, including bandpass variations across the fields, is deferred to Appendix A.

See Sect. 3.7 for a description of particular features that occur in scientific data obtained with OmegaCAM, many of which follow from the properties of the detectors.

### 2.2.2 Auxiliary CCDs

In the periphery of the focal plane OmegaCAM contains four auxiliary CCDs. Two of these are used for guiding (called G1 and G2), both in position and position angle of the field. The other two are mounted out of focus (one is 2mm in front of the focal plane, one 2mm behind). Analysis of pairs of defocused images from these CCDs allows optical aberrations (defocus, coma, astigmatism, ...) to be measured and the telescope to be kept in focus.

## 2.3 Filters

The filter exchange mechanism (Fig. 10) selects filters from two magazines located either side of the focal plane inside the instrument, and slides these into the beam. Each magazine can store six filters. Filter positioning is repeatable to very high accuracy resulting in less than 0.3% rms flux variations between flat fields taken at different times. The footprint of a stellar image is about 1cm in size.

The available filters are listed in Table 3. Transmission curves as measured in the lab are included in Appendix A.

The filters are sandwiches of glass substrates, ca. 14mm thick. Each filter has a baseplate (usually made of BK7) which provides the mechanical support and mounting to the filter frame. Further layers

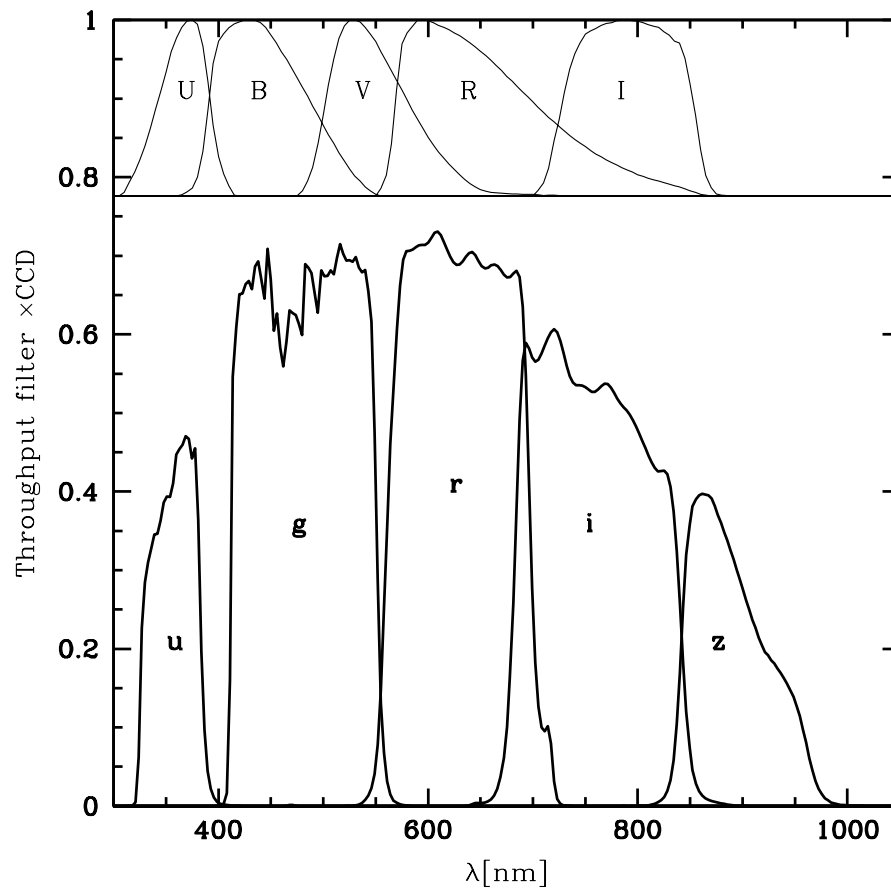


Figure 9: Throughput of the OmegaCAM Sloan filters, times the average quantum efficiency of the CCDs. For comparison, standard (normalised) Johnson-Cousins UBVRI filters are also shown.

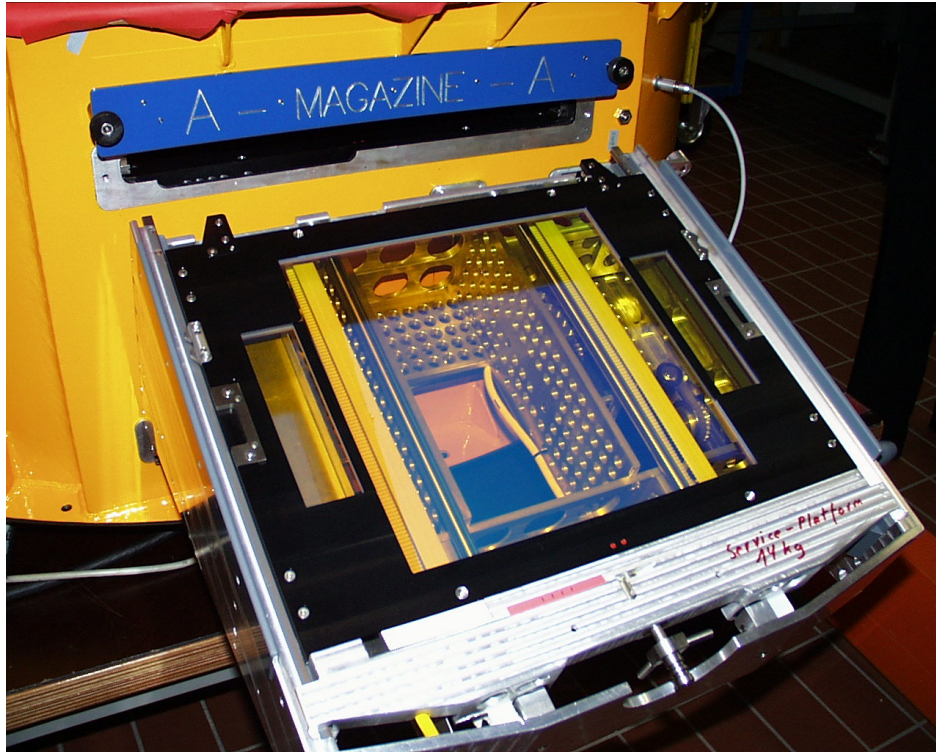


Figure 10: A single OmegaCAM filter ready to be loaded into the instrument. Note the separate filters covering the auxiliary CCDs.

of glass are glued onto this base plate, and provide the filter bandpass, either through coating or by means of coloured glass. For the segmented filters B, V, and NB.659, these layers consist of four quadrants, and the interface of the quadrants casts a slight shadow in the form of a cross onto the image plane (Fig. 11). This central vignetting cross covers  $\pm 310''$  in X and Y direction. In a science observation (Sect. 3.1.1) it can therefore be dithered out with a dither amplitude of  $310''$  in both X and Y.

Most of the narrow-band filters consist of quadrants where each quadrant has a different bandpass. By offsetting the telescope in half-degree steps, and/or rotating the instrument through multiples of 90 degrees, the full field of view can be exposed in all four bandpasses. Which CCD was exposed with which filter segment depends on the magazine the filter is loaded in - this is recorded in the image FITS header (see below, Note on filter magazines).

The auxiliary CCDs, used for guiding and image analysis, are covered by separate filters. Usually these have nearly the same bandpass as the main science filter, but in some cases (the narrow band filters and the u band filter) they are different, in order to boost sensitivity and increase the number of guide stars that can be used.

The Calibration filter is used to observe standard star fields in four bands simultaneously, and hence to monitor variations in the atmospheric extinction throughout the night. For this purpose a specially calibrated standard star field near the South celestial pole has been established (see Sect. 4.1).

### 2.3.1 Note on filter magazines

Because the filter frames can only mate with the filter insertion mechanism on one side, the orientation of a filter with respect to the CCD mosaic depends on the magazine in which it was stored (see Fig. 12). During observations the filter exchange mechanism always returns a filter to the magazine (and slot

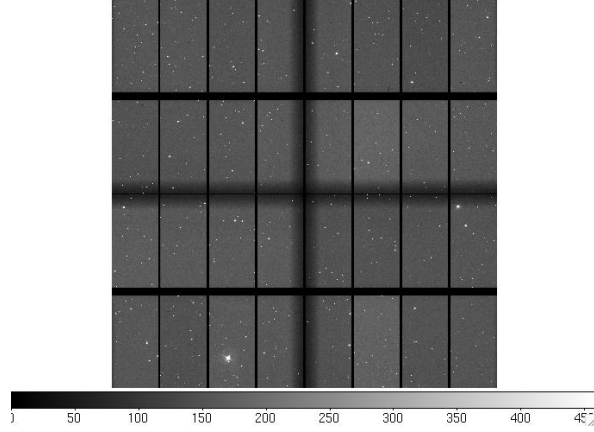


Figure 11: The shadow cast by the cross that separates the different segments of a composite filter (here the V filter).

Table 3: Filters available in OmegaCAM

Filter name	System	$\lambda$ (nm) <sup>a</sup>	$\Delta\lambda$ (nm) <sup>b</sup>	P2 name	comment <sup>c</sup>
$u'$	SDSS	354	56	u_SDSS	IF, M
$g'$	SDSS	475	134	g_SDSS	IF, M
$r'$	SDSS	625	135	r_SDSS	IF, M
$i'$	SDSS	756	155	i_SDSS	IF, M
$z'$	SDSS	880	80	z_SDSS	IF, M
$B$	Johnson	439	103	B_JOHN	IF, S
$V$	Johnson	551	98	V_JOHN	IF, S
$v$	Strömgren	412	21	v_STRM	IF, M
$H\alpha^d$ VPHAS+	—	658.6, 659.3	10.5	NB_659	IF, S
$H\alpha^e$	—	659.0, 666.0, 672.6, 679.1	11	H_ALPHA	IF, 4Q
$H\alpha(z = 0.3)^f$	—	851.9, 861.4, 869.0, 877.7	12.5	NB_852.861.869.878	IF, CG, 4Q
NB3 <sup>f</sup>	—	453.6, 494.3, 533.5, 575.6	15–20	NB_454.494.533.575	IF, CG, 4Q
NB4 <sup>f</sup>	—	616.1, 710.2, 755.1, 816.4	13–20	NB_617.710.755.817	IF, CG, 4Q
Calib <sup>g</sup>	SDSS	$u', g', r', i'$		u_g_r_i_SDSS	IF, CG, 4Q

<sup>a</sup>Central wavelength and <sup>b</sup>FWHM of filter throughput  $\times$  mean CCD QE curve

<sup>c</sup>IF=Interference Filter; CG=Coloured Glass filter; M=Monolithic; S=Segmented; 4Q=4 quadrants with different passband.

<sup>d</sup>This is a private filter for the VPHAS+ survey. Note the slightly different central wavelength of one of the segments.

<sup>e</sup> $H\alpha$  in four slightly overlapping redshift ranges:  $z = 0, 0.01, 0.02, 0.03$ .

<sup>f</sup>These are private filters for use by Munich University Observatory for the first five years of OmegaCAM operations. **Note that these are not currently mounted.**

<sup>g</sup>Because of the different manufacturing processes, the Calib filter bandpasses differ in detail from the monolithic filters.

For the filters consisting of different quadrants, the layout of the quadrants on the sky is as shown below when the filter is inserted in magazine A (for the default orientation of the instrument with PA=0, North is up, East to the left). If the filter is mounted in magazine B the orientation is rotated by 180 degrees.

$H\alpha$	$H\alpha$ VPHAS+	$H\alpha(z = 0.3)$	NB3	NB4	Calib
679 673	658.6 658.6	852 869	494 454	710 616	$u'$ $i'$
659 666	659.3 658.6	861 878	533 576	816 755	$g'$ $r'$

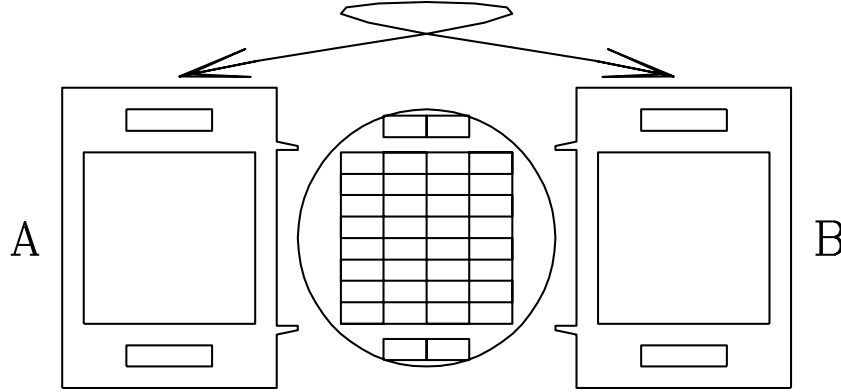


Figure 12: Orientation of a filter depends on whether it is loaded in magazine A or B.

Magazine A	Magazine B
u	opaque
r	g
z	i
V	B
v	Halp
calib	NB659

Table 4: Current OmegaCAM filter distribution. The opaque filter is required to protect the instrument when it is not in operation.

within that magazine) it came from. However, it may happen that a filter needs to be moved manually from one magazine to the other during daytime operations. This flips the orientation of the filter by 180 degrees.

Manual filter manipulations should always be followed by the taking of a new set of flat fields, but if for some reason old flats need to be used it is important to check that these were taken with the same filter orientation. Which magazine a filter was loaded from is logged in the image headers (keyword `INS.FILT1.NO`: magazine ‘A’ contains filter positions 1–6; magazine ‘B’ positions 7–12). Changing from one filter to the next is faster when the filter is in the opposite magazine, since this allows to perform parallel motions of both filters (inserting one, removing the other one). The typical time for filter exchange is one minute for filters between different magazines, and two minutes for filters in the same magazine. See also Table 9 which lists the OmegaCAM observing overheads.

The current order in which the filters are stored in the instrument is shown in Table 4. This order tries to anticipate the typical sequence of filter changes within OBs. It is currently optimised for the sequence  $u'-g'-r'-i'-z'$ .

### 2.3.2 Providing Private Filters

It is possible, but not simple, to use private filters with OmegaCAM. There are a number of constraints:

1. The filters need to be mounted in special frames. These frames grab the filters by the baseplate, which needs to be approx. 5mm thick. Spare frames exist.
2. Overall optical thickness should be equivalent to 15mm fused silica.
3. The costs of these large filters are high (50-100 kEuro), and manufacturing times long (up to a

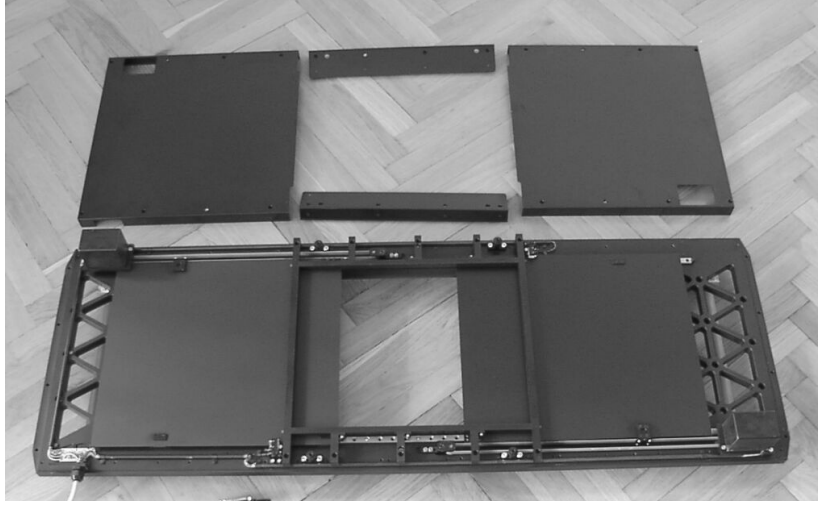


Figure 13: Picture of the partly disassembled shutter unit (Bonn shutter). The two blades, as well as the central aperture, are visible in the lower part of the unit.

year or more).

People interested in using private filters with OmegaCAM should contact the ESO User Support Department ([usd-help@eso.org](mailto:usd-help@eso.org)).

## 2.4 Shutter

The shutter of OmegaCAM is located on top of the instrument, in front of the filters. When closed it covers all 36 CCDs (science + auxiliary). It is a low-acceleration, twin-blade photometric shutter of aperture  $370 \times 292$  mm. The leading blade exposes the CCDs, the trailing blade covers them again. By ensuring that both blades travel with the same acceleration profile the exposure is kept homogeneous over the full beam. For very short exposures (below 0.8 s) the trailing blade starts its motion before the leading blade has finished moving. Over the science CCDs the blades move at constant speed.

Even for exposures as short as 0.1 seconds, the homogeneity over the field is better than 1%. However, it is important to realize that exposures are not simultaneous: there is a lag of about 0.5 second between the exposures at the leading and trailing edge of the field. For high timing accuracy observations, the delay time

$$t_{\text{delay}} = 0.39 + 0.00174X \text{ seconds} \quad (1)$$

needs to be added to the absolute time of the exposure start and end. Here,  $X$  is in mm with respect to the center of the detector mosaic (1mm=14.3 arcsec), and runs along the short sides of the CCDs in the direction of motion of the blades.

Tests during late 2016 indicated that for exposure times of 4ms then no light was arriving on the detectors, at least for CCD number 20. The accuracy of the shutter (two plates) moving over the detector plane sets a limit to the meaningfulness of the integration times below around 1s. The lower the integration time the less accurate it is. For detector 20 for this test the ratio of counts for 32ms compared with a 2056ms exposure was within 2 plus or minus 3 percent of the expected ratio of 1/64.25. Figure 14 shows how the counts changed with exposure time for detector 20.

In case of doubts please get in touch with USD.

The signs of the header keywords DET SHUT TMCLOS and DET SHUT TMOPEN record from which direction the shutter was opened. After the initialisation/reset of the shutter it is always the

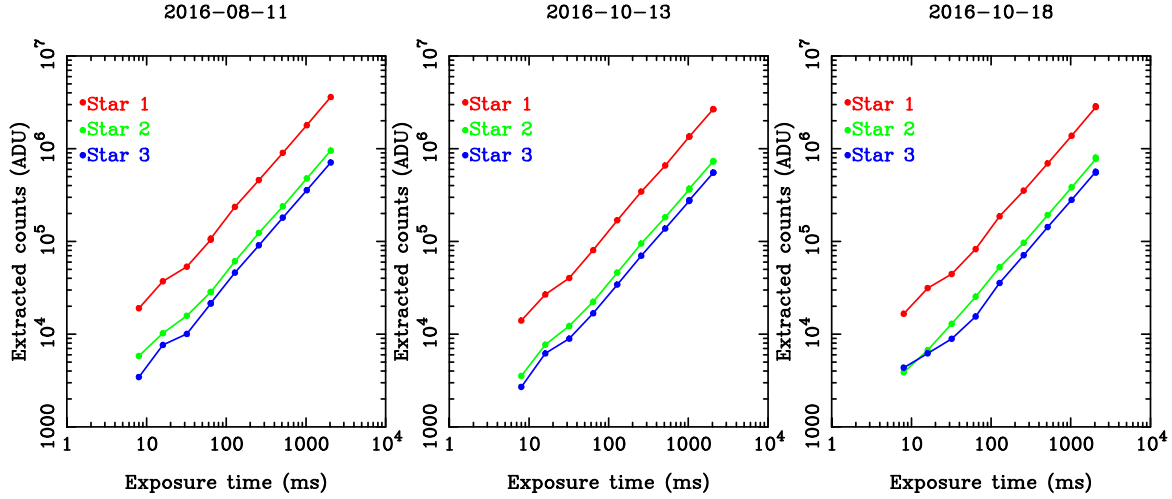


Figure 14: Extracted counts against exposure time for the three stars on CCD 20. We do not plot exposure times of 1-ms, 2-ms and 4-ms as there were no stars visible on these frames even though they should have been detected.

same blade that covers the mosaic, no matter what the previous state was. This blade is defined as BLADE 1 and the blade outside the aperture as BLADE 2. BLADE 1 is at the +x side of the instrument. For the first exposure in a new sequence, BLADE 1 will move outside the aperture and after the exposure time BLADE 2 will move into the aperture. For the next exposure BLADE 2 will uncover the aperture and BLADE 1 moves in again after the exposure is over. The sign of the header keywords are therefore related to the shutter motion in the following way: Blade 1  $\rightarrow$  Blade 2 implies a *positive* value of DET.SHUT.TM keywords. Blade 2  $\rightarrow$  Blade 1 implies a *negative* value of DET.SHUT.TM keywords.

Note that the shutter blades are quite far from focus: at the shutter location the light from a given star is smeared out over a width of about one tenth of the full shutter aperture. This means that the time over which a given pixel receives photons is longer than the actual exposure time, by an amount of roughly 0.08 s. Seen from an individual pixel the photon rate over time does not have steep edges but is smeared out.

## 2.5 Auto-Guiding and Focussing

Both the VST and OmegaCAM contain systems for auto-guiding and for focussing. Focussing happens automatically through real-time sensing of the wavefront. (Filter-dependent focus offsets are also automatically applied.) Traditional through-focus sequences are only needed to calibrate these auto-focus systems.

The VST tracks well, and for exposures shorter than 60 sec there is no need to auto-guide. Depending on the user's image quality requirements, up to 2 minutes without guiding can be accepted, if the target never approaches the zenith to closer than 10 degrees. Commissioning and verification tests have shown that tracking drifts are of order  $\sim 0.1$ - $0.2''$  per minute, but increase when the telescope approaches zenith. Whether autoguiding is desired or not can be specified in the acquisition template of an Observation Block.

### 2.5.1 VST Guide Probe

The VST contains a guide probe with a pick-off mirror, which can patrol the field in front of the filters. It can be used for guiding the telescope and for its active optics system. When required, the probe can be used in between scientific exposures to measure the optical image quality by means of a Shack-Hartmann analysis. This information can then be used to configure the telescope's active optics system.

The probe can in principle also be used for autoguiding and image analysis during scientific exposures. However, unless a suitable guide star exists very close to the edge of the field, the probe vignets the field of view. Use of the OmegaCAM guide and image analysis sensors is thus the default way of operating OmegaCAM and VST. It also avoids the need to move the VST probe in and out of the field, which takes several minutes.

### 2.5.2 Auto-guiding with OmegaCAM

Two guider CCDs are mounted diametrically opposite to each other, near the edges of the field (see Fig. 3). Auto-guiding is done simultaneously on two stars, one on each guider CCD. Guiding with two stars allows field center and rotation to be tracked during an exposure. When the shutter closes, the guider CCDs are not exposed to the sky, and guiding cannot take place. Acquisition of the two guide stars, one per CCD, is designed to happen automatically. If after a readout a second exposure is taken of the same field, the guide stars are re-acquired once the shutter is reopened. If there was no offset commanded for this new exposure, then the auto-guiding will attempt to return the guide stars to the same pixels as in the previous exposures. If an offset is commanded, the auto-guiding will simply keep the stars on the pixels where they are found in this new exposure (i.e., the system does not calculate to which pixels the telescope offset should have sent the stars, but rather assumes that the offset was applied correctly). Telescope offsets that are sufficiently small to keep the guide star on its CCD are accurate to at worst 1 arcsec.

### 2.5.3 Differential Guiding

For observations where non-siderial pointing is required, e.g. to follow or search for solar system objects, the telescope can be given a differential tracking rate. It is currently not possible to guide in this mode, either with the VST guide probe or with OmegaCAM. **Differential Guiding has not been fully commissioned and is not offered for the observing periods P88 and later..**

### 2.5.4 Image Analysis with OmegaCAM

The other two auxiliary CCDs are mounted out of focus, see Figs. 3 and 5. They intersect the stellar light beams in two planes, one in front of, and one behind, the focal plane. This gives information on the deviation of the beams from perfect cones with apex in the focal plane. Different kinds of aberration result in different shapes for these defocused stars, and this can be used to calculate corrections to be applied to the VST's active primary and secondary mirrors. Acquisition of the two image analysis stars, one per CCD, is designed to happen automatically, as does the computation of aberration coefficients. Image analysis is performed at the same wavelength as the autoguiding, which in most cases is the same as the science filter (see Sect. 2.3).

Image Analysis in the acquisition typically requires 3 iterations of 40 seconds each. During science exposures, aberrations are constantly measured by the IA system, and corrections are applied to the mirrors during the readout. The minimum science integration time that guarantees at least one aberration measurement is about 1 minute. OBs with shorter science exposures will not get additional IA corrections after the acquisition. Tests have shown that the IQ remains reasonably stable for about



half an hour without IA corrections. OBs that consist of short integration times should therefore not last more than half an hour. Image Analysis in the acquisition can be disabled for concatenations of short OBs that perform a sequence of observations back-to-back in adjacent fields.

### 2.5.5 Traffic rules between science and auxiliary CCD readouts

The OmegaCAM CCDs are controlled by three controllers (called FIERA 1/2/3), where FIERAs 1 & 2 control the science CCDs, and FIERA 3 the auxiliary CCDs (Fig. 3). FIERA1 is the master controller (Fig. 7). The readout rules are such that the science array cannot be read out at the same time than the auxiliary CCDs. Otherwise, strong interference noise patterns will appear in auxiliary and science CCDs. Therefore, the AG and IA loops always stop about 10 seconds before the end of each science exposure.

Furthermore, upon science CCD readout, the OmegaCAM shutter is closed, such that no light falls on the auxiliary CCDs either. AG and IA are therefore always paused from 10s before the end of a science integration until the start of the next science integration.

## 2.6 Calibration lamps

Dome flat exposures are taken with calibration lamps mounted at  $90^\circ$  intervals on the top ring of the telescope, illuminating a white screen on the inside of the telescope dome. The lamps are operated by carefully controlling the electric current, and their brightness is stable to about a percent over a timescale of several weeks.

Dome flat fields are used for monitoring the small-scale (pixel-to-pixel) variations in sensitivity of OmegaCAM, and for overall system throughput monitoring. Two sets of four lamps each are mounted side by side. One set is used for routine daily calibrations, meanwhile the second set is cross-calibrated against the first at regular intervals. Once the lifetime of the first set of lamps has expired, its role is taken over by the second set, and the first set is replaced with new lamps. This procedure ensures a continuous record of throughput measurements, provides dome flat fields, and serves as a daytime health check.

## 2.7 Photometric Properties

Indicative magnitude zero points (the AB magnitude of a star that generates one electron per second) are given in Table 5. These numbers are consistent with the on-line Exposure Time Calculator (ETC)<sup>1</sup>, which is based on the throughputs and reflectivities of the individual optical components.

Because the angle of light incidence varies with distance from the center, the OmegaCAM filters show some bandpass variation across the field. This variation is mostly axisymmetric, and it introduces a radially dependent colour term. Measurements will be included once they are available.

## 2.8 Astrometric Properties

By design, OmegaCAM and the VST deliver a quite constant plate scale, and a rather uniform PSF. The radial plate scale is constant over the field to better than 1 part in 1000, and independent of the filter used. The pixel scale with ADC in is  $0.215''/\text{pix}$ . With the ADC out – hence two-lens corrector in – it is  $0.213''/\text{pix}$ . From P99 the ADC will not be offered.

<sup>1</sup><http://www.eso.org/observing/etc/bin/gen/form?INS.NAME=OMEGACAM+INS.MODE=imaging>

Filter	Mag zero pt (AB)
$u'$	23.9
$g'$	25.8
$r'$	25.7
$i'$	25.2
$z'$	23.8
$B$	25.7
$V$	25.5

Table 5: Magnitude zero points for the SDSS and Johnson filter sets. These are average values; chip-to-chip scatter is of order 0.1 mag.

## 2.9 Flat fielding of OmegaCAM data / Illumination correction

Both twilight (and to lesser extent dome flats) have a straylight component. This straylight component is centrally concentrated (“sky concentration”) and makes the flatfield exposures overexposed in the center of the FOV. Applying the flatfield exposures without any correction would result in an erroneous apparent trend of photometric ZP with distance from FOV center. The sky concentration hence needs to be corrected for, after flatfielding the data. The corresponding procedure is called Illumination Correction (see e.g. Section 2.8.4. of McFarland et al. 2011, arXiv:1110.2509). For OmegaCAM it consists of taking 32-dither observations of a photometric standard field such that the same group of standard stars is consecutively observed in each CCD. These data is flatfielded with a flatfield that is a combination of the small-scale structure in the domeflat and large-scale structure of the twilight flat. The ZP residuals after flatfielding are then modeled with a 2D-polynomial and 32 ZPs as free parameters. The relevant steps are illustrated in Fig. 15, for the r-band. The illumination correction reaches 15-20% at the very edges of the FOV for all Sloan filters. Indicative illumination correction fitting coefficients, as determined in the commissioning, are shown in Table 6 for the  $u'g'r'i'$  filters.

Filter	Coeff xx	Coeff xy	Coeff yy
$u'$	1.6153389e-09	1.9320844e-10	1.4650246e-09
$g'$	1.7019895e-09	3.3104022e-11	1.6704393e-09
$r'$	1.5453463e-09	2.5500341e-11	1.3853747e-09
$i'$	1.5270148e-09	1.0777857e-10	1.1392408e-09

Table 6: This table gives the polynomial coefficients for illumination correction functions as illustrated in Fig. 16. x,y is in pixel units with x,y=0,0 at the mosaic center. At distances of 10.000 pixels from mosaic center (close to the edge of the FOV), the illumination corrections is around 15%.

An important note must be made in this context: twilight flats have in addition to the rotationally symmetric straylight component an irregular contribution (see Fig. 16). These patterns occur most likely due to the incident angle criterion of the Fabry-Perot throughput of those interference filters. The non-symmetric component is of order 5-8% of the average flux, and as such pose a limitation to accurate flat fielding with sky flats. Moreover, it requires that the science data are flatfielded using twilights flats at the same rotator angle as the flatfield used in determining the illumination correction. The OmegaCAM consortium is therefore investigating alternative approaches, e.g., using only domeflats which appear to have an amplitude of  $\sim 5\%$  or less in the amplitude of the sky concentration.

### 2.9.1 Performances of the new Baffling system

The installation of the new baffling system has been completed during P93. The new baffles are designed to reduce the amount of background brightness as well as the amount of stray-light component in OmegaCAM images. After the installation of the baffling, a number of tests on sky have been performed in order to quantify the amount of background and stray-light removed. In particular the analysis of the ratios between raw dome flatfields taken before and after the new baffling installation

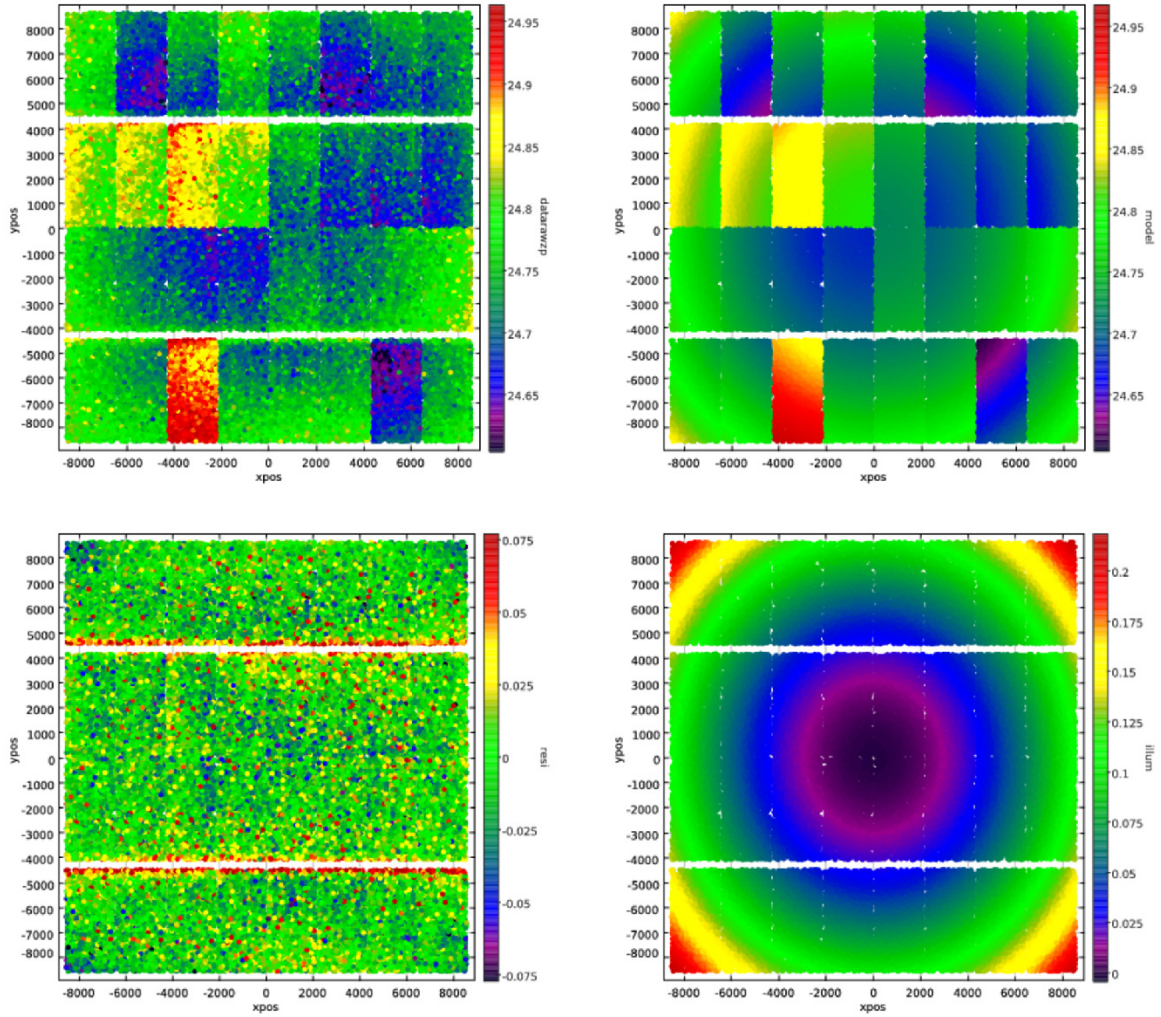


Figure 15: Example of illumination correction derivation for OmegaCAM Sloan r. Input data are 32-dither observations of SA113. The magnitude residuals after flatfielding are modeled with one 2D-polynomial + 32 ZPs as free parameters. SDSS DR7 is used as standard star catalog. Top left: magnitude residuals after flatfielding (ZP per chip are not subtracted). Top right: model. Bottom left: External magnitude residuals after illumination model has been applied. Bottom right: model with uniform ZP, that is with individual ZPs per chip subtracted. The illumination correction reaches  $\sim 0.2$  mag at the edges of the FOV.

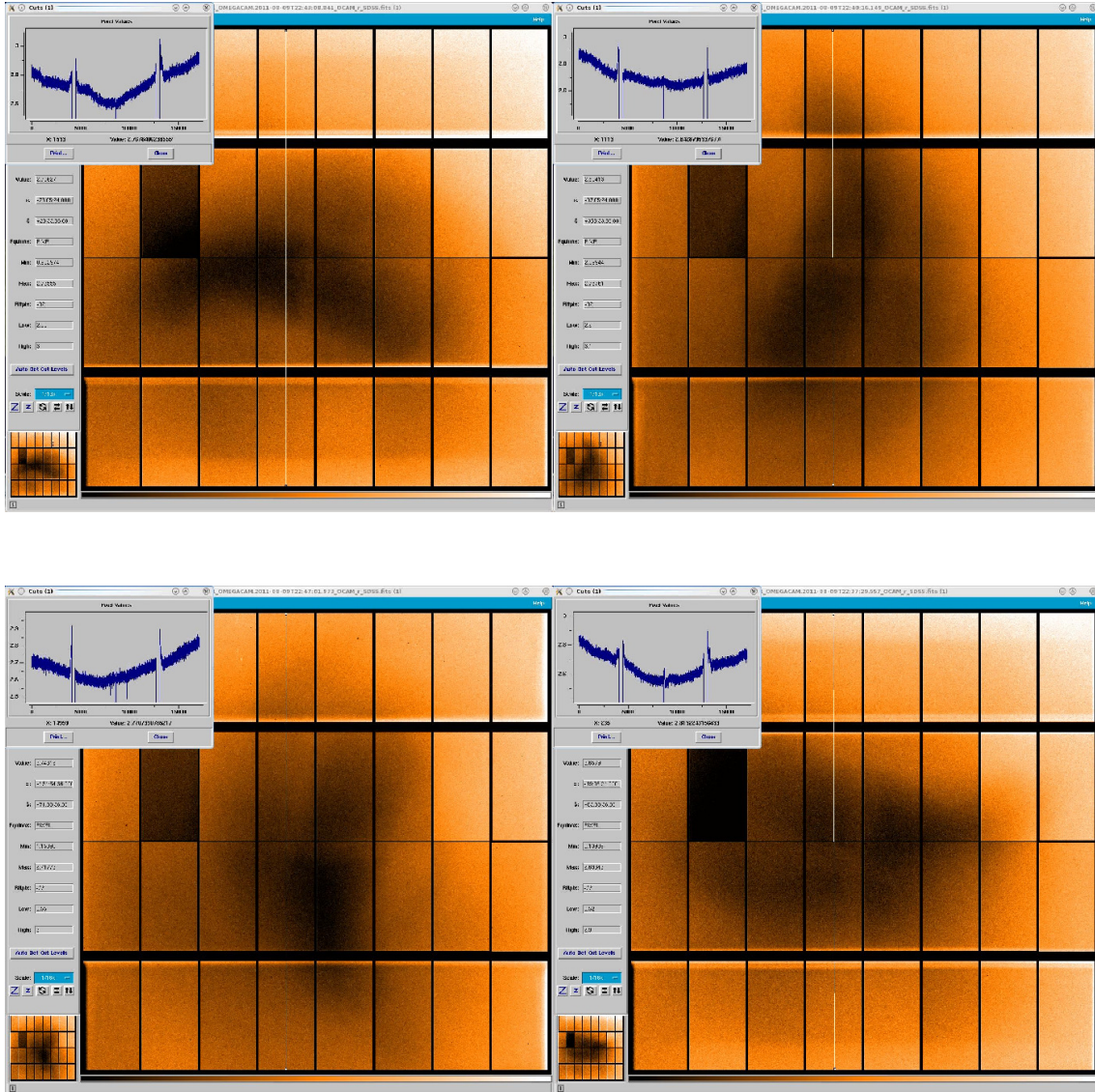


Figure 16: Raw  $r'$ -band dome flat divided by raw twilight flat for four different absolute rotator angles. From top left to bottom right, absolute rotator position angles are  $-107.6$ ,  $-18.3$ ,  $163.1$ , and  $71.2$  degrees. The asymmetric patterns has an amplitude of 5-8%.



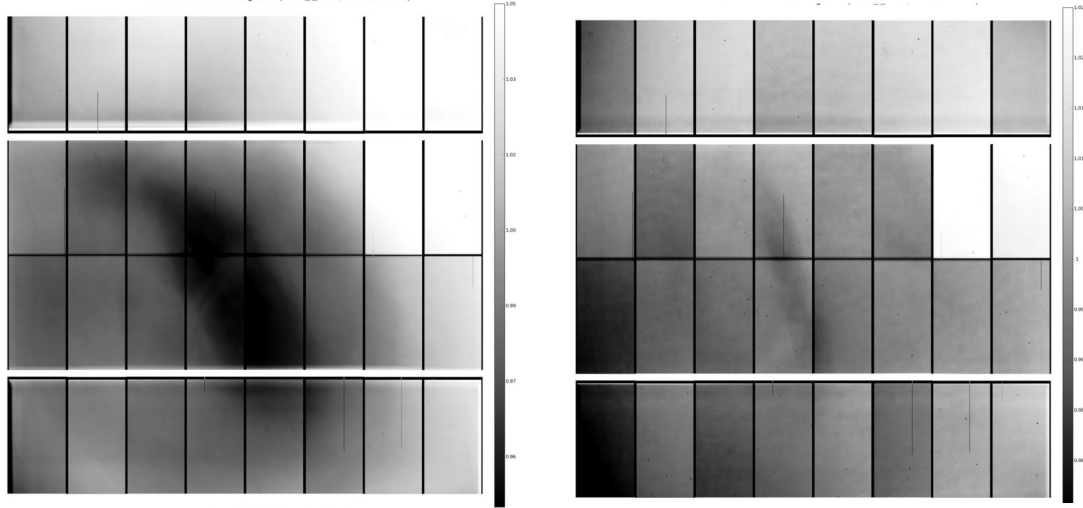


Figure 17: Raw  $r'$ -band dome flat divided by raw twilight flat taken at the same absolute rotator angles before and after the installation of the new baffling system (left and right panel, respectively).

shows that 6% to 8% of light distribution has been removed in all bands. A confirmation is offered by the same analysis performed using the twilights flatfields. Moreover, the ratios of raw twilights flatfields are consistent with M2, chimney and M1 plug together removing foremost an oval/circular stray-light distribution but removing slightly less stray light near CCD edges. Some residual stray-light is still visible after the study of twilights flatfields and with test-observations performed in the vicinity of bright stars and the Moon.

Fig. 17 shows the ratio of raw  $r'$ -band dome flat divided by raw twilight flat, taken at the same absolute rotator angles ( $\sim -137$  degrees), before and after the installation of the new baffling system (left and right panel, respectively). It is visible that dome-to-twilight ratio images are consistent with the presence of residual stray light in the twilight flatfields compared to dome flatfields.

Moreover the residual stray-light component shows an irregular distribution that does not simply rotate with the change of rotator angle but changes morphology as well. As a consequence it remains the case that the domeflats appear ideal to model pixel-sensitivities of science images thanks to having (1) less stray light and (2) stray light in a rather simple circular distribution. The use of twilight flatfields is instead recommended in order to proper model the stray-light in science images.

A specially designed system of ribs will be installed in the new baffling mechanism. The ribs will allow to remove most of parasitic light coming from the Moon, bright stars and the sky. A prototype was positively tested on two nights between June 14/15 and Jun 16/17. The final ribs' system is expected to be installed by the end of 2014.

OmegaCAM users are invited to follow the OmegaCam News page<sup>2</sup> where updated information related to the new ribs' installation will be posted.

<sup>2</sup><http://www.eso.org/sci/facilities/paranal/instruments/omegacam/news.html>

## 2.10 Effect of the laser guide star facility on OmegaCam

During December 2016 tests were performed to determine the effect of the 4 laser guide star facility on OmegaCam. Figure 18 shows OmegaCAM r\_SDSS observations of 60s integration time taken without tracking at low altitude where the laser is out of focus. The Moon was below the horizon. Figure 19 shows a 20s exposure in focus without tracking in r\_SDSS.

The results of the dropoff with counts from the 4LGSF laser in the r\_SDSS band are shown in Figures 20 and 21. At an altitude of around 84 degrees the laser counts are similar to the night sky background in dark time at a distance to the laser of around 1 degree. Finally, Figure 22 shows a 300s observation taken with NB659 followed by a 20s exposure using the r\_SDSS filter, using the old PARLA laser system. No obvious laser light is visible using the NB659, indicating it is laser insensitive to low levels.

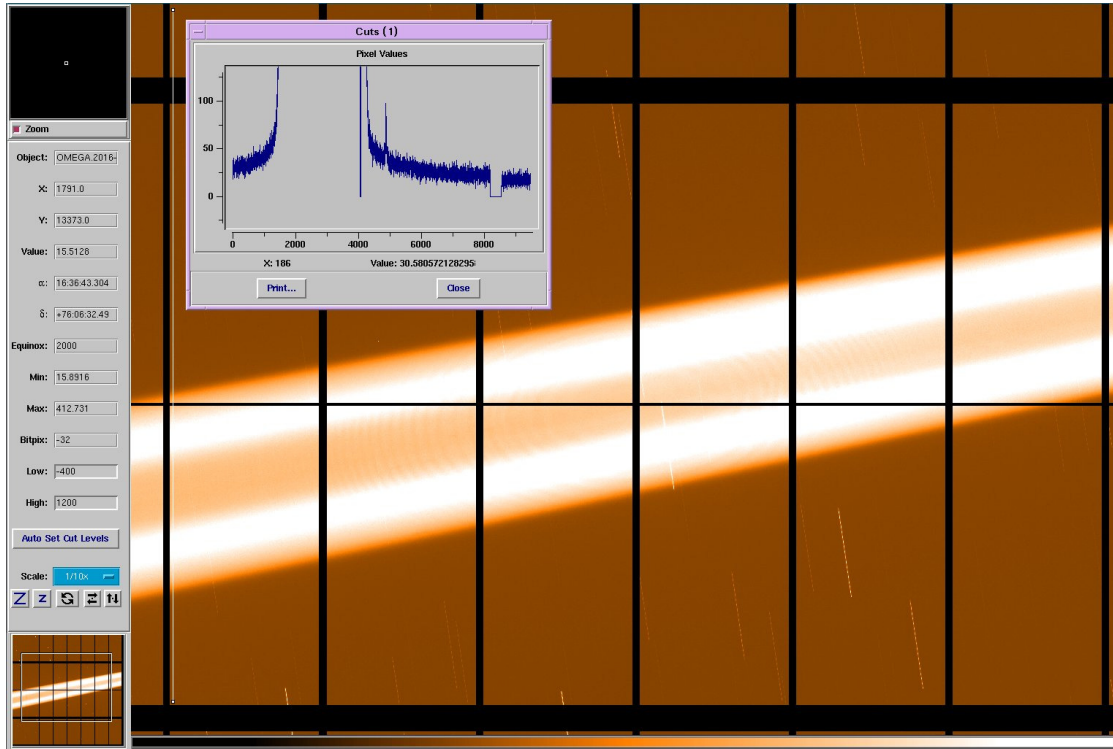


Figure 18: Reduced observations taken in clear conditions with no Moon of the out-of-focus 4LGSF laser with OmegaCAM in r\_SDSS with 60s of exposure time without tracking.

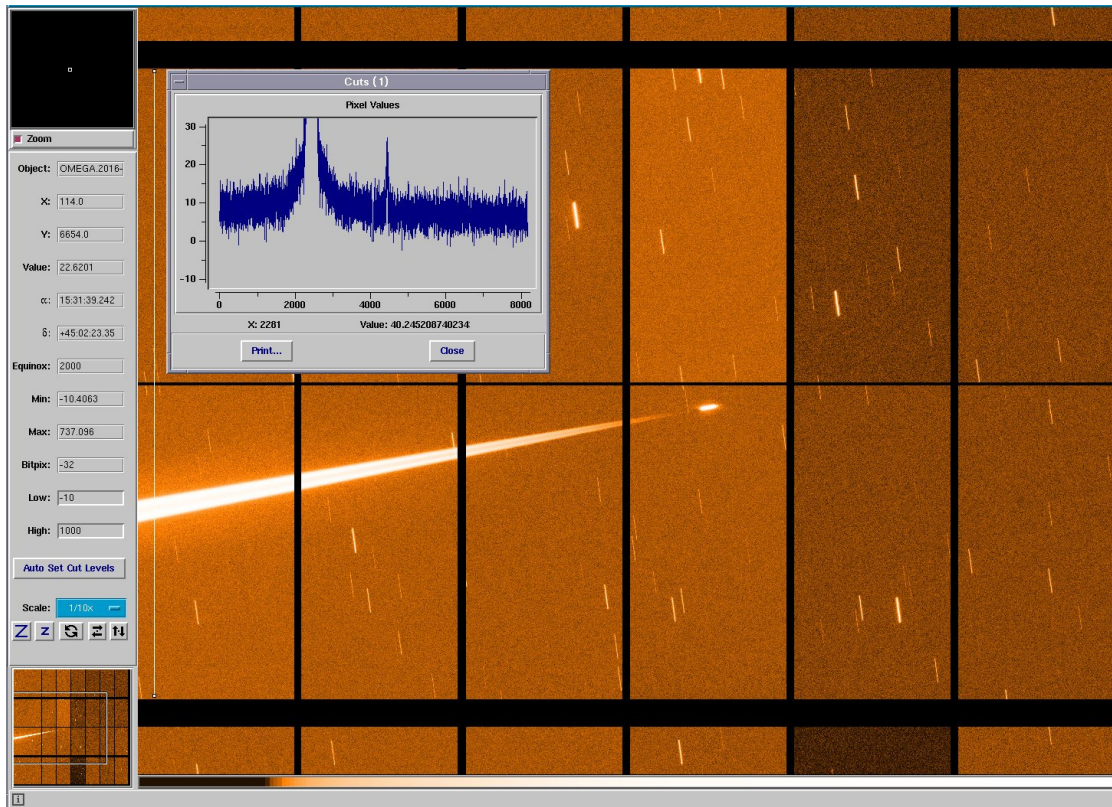


Figure 19: Reduced observations taken in clear conditions with no Moon of the in-focus 4LGSF laser with OmegaCAM in r\_SDSS with 20s of exposure time without tracking.

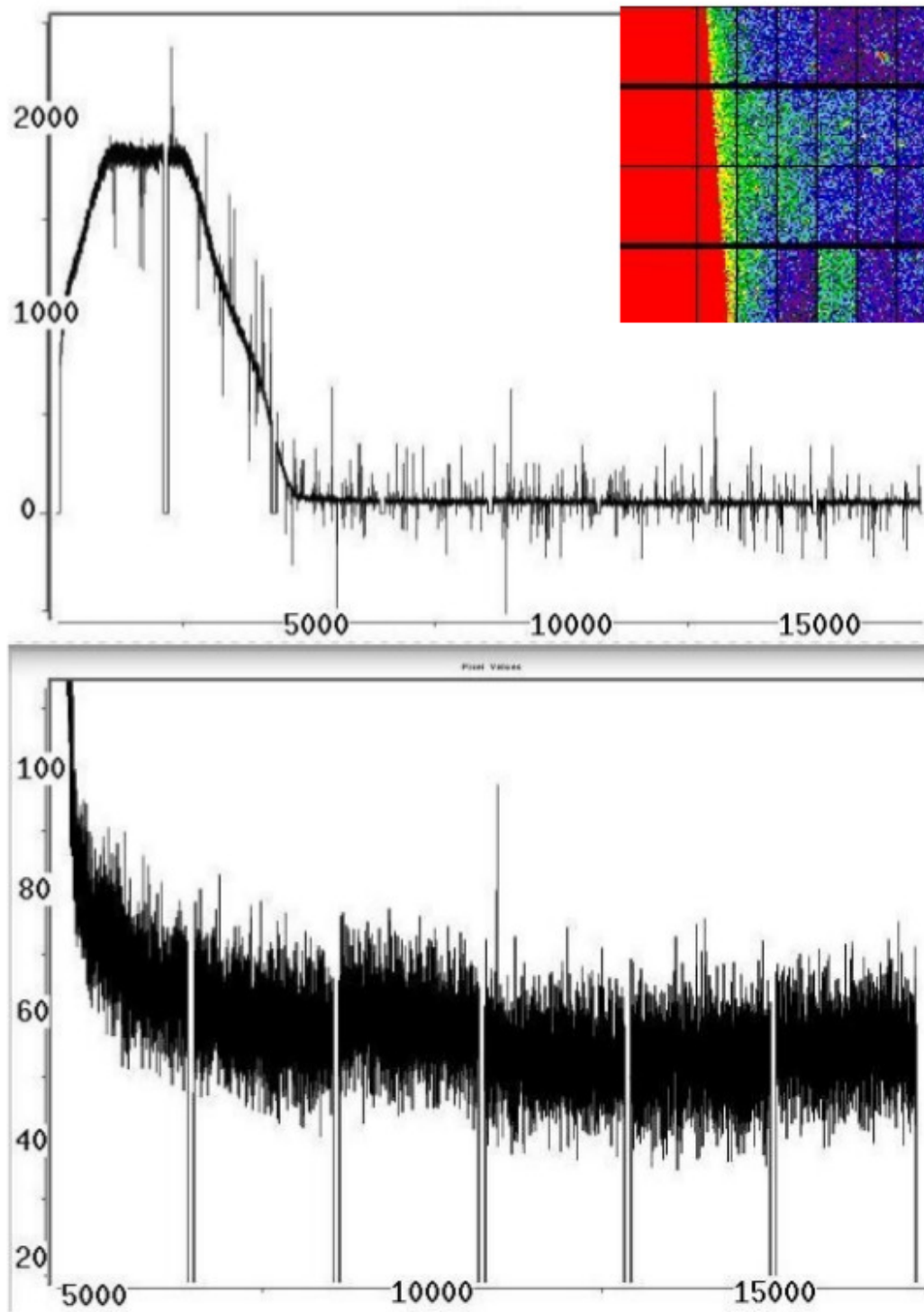


Figure 20: Cut in x at the top of the image across a r<sub>SDSS</sub> 60s exposure (top panel inset, VST altitude=84.375 degrees) where the laser (red) is nearly vertical on the left hand side of the detector array. ADUs per pixel against x distance Note that 15,000 pixels are approximately 50 arcminutes. Top panel: Full range in intensity shown. Bottom panel: Reduced range in intensity. The counts at 50 arcminutes away are approximately 1 ADU per second which are slightly less than that expected just from the sky only value in dark time.



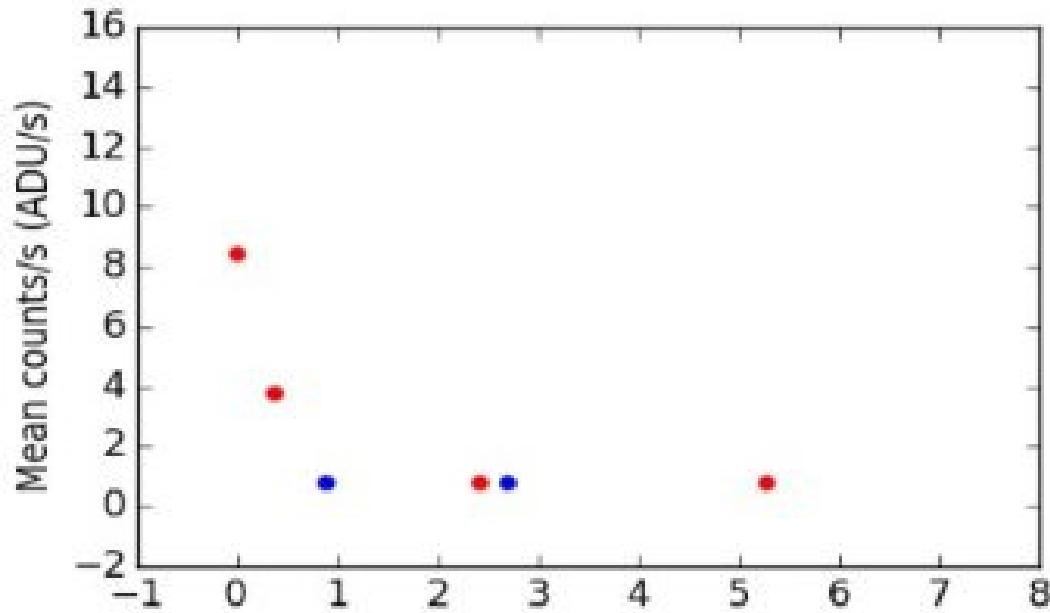


Figure 21: Mean counts in ADU per second against distance from the 4LGSF laser in degrees for observations taken on 2016-12-01T03:39:35 (VST altitude 84.4 degrees). Blue dots were with the laser off with red dots the laser on.

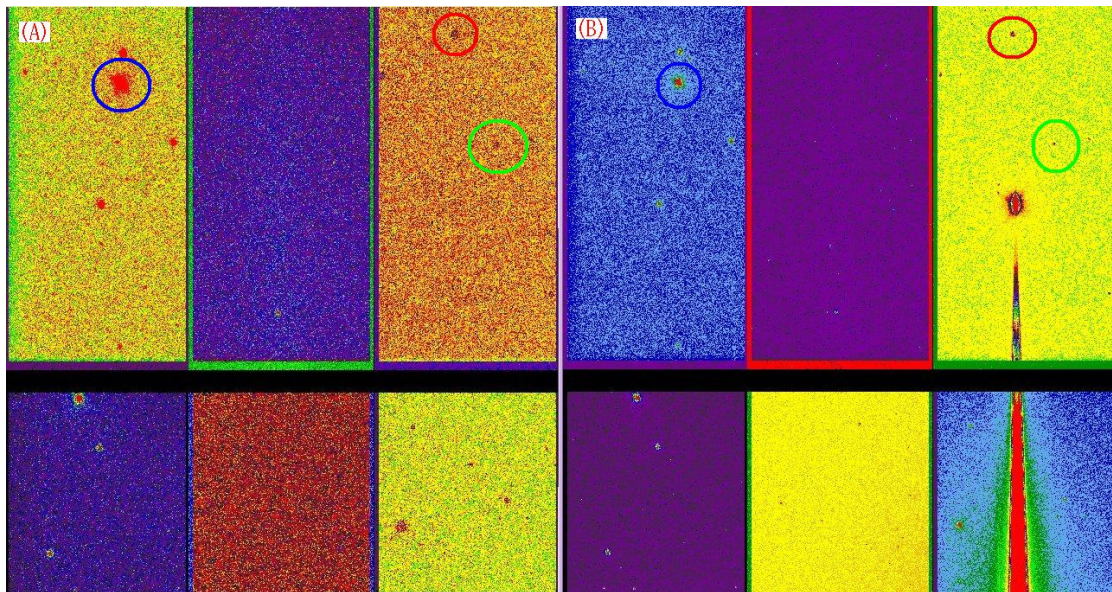


Figure 22: (A) A 300s exposure taken with the NB659 filter and OmegaCAM (B) A 20s exposure taken using the r\_SDSS filter on the same field. In both cases the PARLA laser was propagating (somewhat less powerful than the new 4LGSF system). Blue, red and green circles show stars visible on both images. The images are raw (no reduction has been performed). No laser light is visible when using the NB659 filter.

### 3 Observing with OmegaCAM

To carry out observations with OmegaCAM, users need to prepare Observing Blocks (OBs) before the observations and submit those to ESO, using the Phase 2 Proposal Preparation (P2) tool. More details on how to define OBs are given in Sect. 3.3 and in [RD5]. First the offsetting modes, and the effects of atmospheric refraction and dispersion, are described.

Please consult the ESO call for proposals <https://www.eso.org/sci/observing/phase1.html> for details concerning allowed programmes (normal, monitoring, large etc) that may change period by period.

#### 3.1 Offsetting Modes and Observing Strategies

##### 3.1.1 Offsetting Modes

OmegaCAM observations can be taken with a number of *Offsetting Modes*: STARE, OFFSET, DITHER, or JITTER. They differ in the kind of offsets that are used between exposures, and in the final data product.

1. STARE: A sequence of  $N$  exposures of exactly the same part of the sky (except for the effect of differential atmospheric refraction, see Sect. 3.2.1). No offsets are done. To allow removal of cosmic rays by taking the median of images  $N$  must be at least 3.
2. OFFSET: A sequence of  $N$  exposures with almost full flexibility of offsets. Two limitations are to be considered. 1. Large offsets beyond the default dither pattern (Sect. 3.4.2) increase the overheads due to the need of guide star reacquisition. The execution time for offset sequences therefore increases by about 1 minute for each offset that goes beyond the default dither pattern (P2 takes care of this calculation). This penalty will not apply if guiding is disabled in the acquisition, which is possible for short integrations of 1-2 minutes. 2. The maximum of a single offset accepted by the telescope is 1 degree in each of RA and DEC.
3. DITHER: A sequence of  $N$  exposures with offsets that are sufficiently large to bridge the gaps (up to  $80''$ ) between the CCDs in the detector mosaic. A DITHER observation results in an image which covers the field continuously, without large holes (provided  $N > 3$ ). Some parts of the sky are seen by several CCDs, and all parts of the field are seen in at least  $N - 2$  exposures. A dither amplitude of  $310''$  is recommended to cover the shadow cast by the cross of the segmented filters B, V, NB<sub>659</sub>. See also Sect. 2.3.
4. JITTER: A sequence of  $N$  exposures with offsets that are sufficiently large (of order 1 arcsec) to shift cosmetic CCD blemishes to different parts of the sky. A JITTER observation results in a 32-fragment image (one fragment per CCD) in which the gaps between CCDs remain, but in which any part of the sky is seen by at most one CCD.

The pattern of offsets between successive exposures on a field distinguishes *dither* and *jitter*. They represent different trade-offs between trying to obtain data with uniform exposure level over the full OmegaCAM field, and trying to avoid having areas on the sky where data from different CCDs need to be combined. Such overlaps can give rise to discontinuities in the way the PSF varies across the field in the final stacked image, but this is unavoidable if the full field is to be exposed.

The key differences between the two modes are summarised in Table 7.

A number of patterns have been pre-defined for dither and jitter. They are described in more detail in the Template Manual [RD1].

	<b>JITTER</b>	<b>DITHER</b>
<b>Correct what?</b>	CCD blemishes only	also gaps in focal plane
<b>Offsets</b>	few arcsec	25-100 arcsec
<b>Data product</b>	fragmented 1-square-degree-image	filled 1-square-degree image
<b>Advantage</b>	no combination of data from different CCDs	~homogeneous exposure level
<b>Penalty</b>	gaps between CCDs	possible sharp changes in PSF

Table 7: Key difference between the dither and jitter modes.

Programmes that require very accurate PSF measurements should preferably use *jitter* as it results in a PSF which varies continuously over each CCD (except near the very edges)<sup>3</sup>. *Dither* data should be used if the primary aim is to image a field completely.

### 3.1.2 Observing Strategies

Observations are also taken under different *Observing Strategies*, which are defined in the observing templates in P2. Note that these strategy keywords are ignored in ESO's Data Flow System, but may help the users in their own data reduction. The strategy used is written to the image headers (keyword TPL OBSSTRG).

Strategies extend beyond single OBs. The defined strategies are STANDARD, FREQ, DEEP, or MOSAIC. They can relate to how fields are laid out during observation preparation, and they can also provide specific instructions for data reduction, and for scheduling.

1. STANDARD: Used for a stand-alone OB, with no particular relation to other observations.
2. DEEP: Observations intended to generate a deep image, built up over several (typically many) OBs.
3. FREQ: Observations in which a field is monitored to form a time series. Specific time links (from minutes to months) may be specified for such observations as part of the OB preparation in P2. Specific time intervals can be specified for each OB; complex scheduling constraints, e.g. 'observe OB 1 five days after OB 2', can be specified in P2 via time-links.
4. MOSAIC: Observations which will be used to map an area of the sky consisting of several (typically many) adjacent pointings.

## 3.2 Atmospheric Refraction and Dispersion

The atmosphere refracts light, as a result of which sources appear slightly closer to the zenith than they would be without the atmosphere. The effect is slightly wavelength dependent. This has two consequences: *atmospheric refraction* and *atmospheric dispersion*.

### 3.2.1 Atmospheric Refraction

A star's extra displacement  $r$  towards the zenith due to atmospheric refraction is given by

$$r = R \tan Z \quad \text{rad} \quad (2)$$

where  $Z$  is the zenith distance of the star, and  $R$  is the refractive index of air minus 1. To a good approximation

$$R \simeq 1 \text{ arcmin}. \quad (3)$$

<sup>3</sup>Note that, even though the CCD mosaic is extremely flat, significant jumps in PSF can still occur in coadded dithered images if the seeing varies from one exposure to the next.

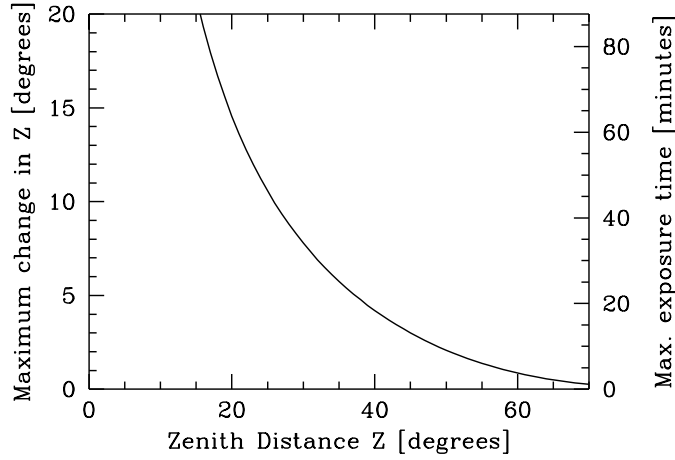


Figure 23: The maximum change  $\Delta Z$  in zenith distance (degrees) that is allowed during an exposure before the image quality is degraded by 0.1 arcsec due to atmospheric refraction. The right-hand axis approximately translates this limit into an exposure time  $T$  (minutes) for a field on the equator, as seen from the Paranal latitude of  $-24^\circ$ :  $T = 4\Delta Z / \cos(-24^\circ)$ .

( $R$  is slightly wavelength-dependent: see Sect. 3.2.2.)

Over the field of OmegaCAM,  $r$  takes slightly different values: from the center to the edge  $Z$  differs by  $\delta Z = 0.5^\circ$ , and so  $r$  varies by

$$\delta r \simeq R \sec^2 Z \delta Z \simeq 0.5'' \sec^2 Z. \quad (4)$$

Thus, the size of the field changes with zenith distance by an amount  $2\delta r \simeq 1.0'' \sec^2 Z$ . This is not a concern since the astrometric standard stars in the field suffer the same refraction, and so this effect is taken out in standard data reduction.

However, atmospheric refraction does affect long exposures at lower elevations. If  $\delta r$  changes significantly during an exposure then it becomes impossible to track objects in the center and outer parts of the mosaic at the same time (guiding with two stars will favour the center). As a result, image quality in the outer parts of the field will be degraded. The way to prevent this is to keep the exposures short, and so avoid a large change of  $\delta r$  during an exposure.

For  $\delta r$  not to change by more than 0.1 arcsec over an exposure requires

$$\delta(0.5'' \sec^2 Z) < 0.1'' \quad \text{or} \quad \delta Z < 6^\circ \cot Z \cos^2 Z. \quad (5)$$

At  $Z = 45^\circ$ , therefore,  $Z$  must not change by more than 3 degrees per exposure (for a target near the celestial equator this means no more than 12 min exposure); at  $Z = 60^\circ$  the limit is below a degree change allowed (4 min exposure).

In poor seeing, or if image quality constraints are not so stringent, this limit can be relaxed and presents no practical concern.

Figure 23 shows a plot of the limit given by eq. 5.

### 3.2.2 Atmospheric Dispersion

Because refraction is wavelength dependent (more strongly so in blue light), the atmosphere turns objects into little spectra with the blue end pointed at zenith. Within the bandpass of a broad band filter

Filter	Airmass at which dispersion reaches		
	0.2 arcsec	0.5 arcsec	1 arcsec
$u'$	1.05	1.22	1.75
$g'$	1.05	1.20	1.65
$r'$	1.20	1.90	3.35
$i'$	1.30	3.40	> 5
$z'$	2.40	> 5	> 5

Table 8: The airmass (sec  $Z$ ) at which the length of the atmospheric dispersion induced ‘spectrum’ reaches 0.2, 0.5 and 1 arcsec, for the SDSS filters.

this can cause image elongation and degradation. A model for the amount of atmospheric dispersion on Paranal has been calculated by E. Marchetti, see <http://eso.org/gen-fac/pubs/astclim/lasilla/diffrefr.html>. Based on these data, Table 8 shows the airmass at which atmospheric dispersion causes a smearing of the light over a 0.2 arcsec (1 pixel), 0.5 and 1 arcsec length. It is the responsibility of the user to specify the airmass constraints of their observations as a function of the filter used and the image quality requirements.

To compensate the atmospheric dispersion effect, an Atmospheric Dispersion Compensator (ADC) was designed for the VST. It consists of two sets of counter-rotating prisms with which one can introduce given amounts of dispersion and thus cancel the atmospheric dispersion. The ADC has good throughput longward of 360nm wavelength; unfortunately this does not include the  $u'$  band<sup>4</sup>.

**Important Note.** The ADC was not fully characterised and commissioned yet (P90). Therefore, it is not offered and will be removed from templates in P99.

### 3.3 OB preparation

Preparing an Observing Block for OmegaCAM is done with ESO’s P2 tool[RD5]. An OB consists of a number of templates, each of which represents a standard action taken by the telescope and/or instrument. Each OB must include one *target acquisition template*, whose main role it is to point the telescope at the target, and one or more *science templates* which perform the actual observation. In addition an OB contains a *constraint set* which specifies under which conditions (image quality, transparency, moon phase, precipitable water vapour, timing constraints, ...) the OB may be executed. Full details are given in the P2 instructions on the ESO web site [RD5].

For reasons of flexible scheduling of service mode observations at ESO and to increase the chances that an OB is executed fully within constraints, the total execution time of each OB must be at most one hour. Longer observations need to be split into separate OBs. Unless there are good reasons to do otherwise, OBs should only use one filter each. If filter changes inside an OB are required, it is most efficient to order the exposures in such a way that filters are alternately selected from the two magazines. See Table 4 for the filter distribution.

To help with planning observations, one can use the Exposure Time Calculator (ETC) from the ESO web site. Starting in P105 turbulence categories are used instead of seeing.<sup>5</sup>

#### 3.3.1 Target acquisition

A target acquisition presets the telescope pointing and configures the mirrors, corrector and instrument rotator. In addition it simultaneously prepares the instrument by loading the appropriate filter in the beam, and acquiring guide stars and image analysis stars if required.

<sup>4</sup>Note that the atmospheric extinction in  $u'$  is high, so observations in this band should in any case be taken as close to zenith as possible.

<sup>5</sup><http://www.eso.org/observing/etc/bin/gen/form?INS.NAME=OMEGACAM+INS.MODE=imaging>

### 3.3.2 Scientific exposure

The scientific exposures load an appropriate filter, lock onto the guide and IA stars, perform any offsets, clear the CCD array, open the shutter for the appropriate time, close the shutter and read out the CCD array. A science template may command a number of exposures, possibly interspersed with offsets. Within a template, parameter lists are cycled through if the number of values is smaller than the number of exposures specified. Several science templates are needed if consecutive observations with different filters are required.

### 3.3.3 Dither and jitter patterns

Different templates are used for observations taken in dither or jitter mode. These templates implement different default offset patterns. The patterns are described in the Template Manual [RD1].

## 3.4 The Observing templates

The detailed use of the templates is described in a separate document [RD1]. Here the main functionality of the available templates is described.

### 3.4.1 Target Acquisition Templates

Each OB must start with an acquisition template, whose execution points the telescope and prepares the instrument.

Two acquisition templates are provided: `OMEGACAM_img_acq` and `OMEGACAM_img_acq_movetogap`. Each acquisition template allows specification of the object position, instrument filter for the first exposure, ADC or two-lens corrector (settings `COORD` and `NONE`, respectively), and Cassegrain rotator offset angle. The ADC is not offered and will be removed from templates in P99. It is also possible to specify whether or not autoguiding is required. Based on experience so far, unguided tracking for 60 seconds does not degrade image quality measurably. Finally, for OBs in concatenation it is possible to disable the start of Image Analysis in the acquisition.

The difference between `OMEGACAM_img_acq` and `OMEGACAM_img_acq_movetogap` is that the former acquires the field ‘blind’, while the latter takes a short exposure, which the operator can display and use to move the telescope so that a selected bright star falls in a gap between CCDs in order to reduce reflections and remanence.

### 3.4.2 Science Templates

Science templates perform the actual scientific exposure. For each of these templates the user must specify the exposure time and the filter to be employed, and optionally, the Observing Strategy used (see Sect. 3.1.2). The templates differ in the number and pattern of offsets that they use.

`OMEGACAM_img_obs_stare` takes a number of exposures through the same filter. The number of exposures, and the exposure time are specified. No offsets are made.

`OMEGACAM_img_obs_jitter` performs a jittered exposure (see Sect. 3.1.1). The number of exposures, the exposure times, and the step size for the jitter pattern can be specified. A step size of 1 arcsec suffices to correct for CCD blemishes and most dust particles on the detectors. If it is required that a given source is seen by a completely different set of pixels in each sub-exposure, the step size needs to be increased to above that of the sources. This is particularly true if accurate, real-time fringe maps need to be derived from the observations themselves. In those cases *dithering* may be more

appropriate.

The jitter template allows step sizes up to 100 arcsec but such large offsets are not recommended.

`OMEGACAM_img_obs_dither` performs a dithered exposure (see Sect. 3.1.1). The number of exposures, the exposure times, and the step size for the dither pattern can be specified. The dither patterns are designed to make sure the full field is observed, without gaps. Two step sizes can be given, one in  $X$  (along CCD rows) and one in  $Y$  (along columns). It is recommended that these are set to 25 and 85 arcsec, respectively, which are slightly larger than the largest gaps in the mosaic. Exceptions are the segmented filters B, V, and NB\_659, for which the step sizes should be 310'' in both  $X$  and  $Y$ , to dither out the shadowing by the filter cross (Sect. 2.3).

Two dither patterns are provided. The 'diag' pattern simply offsets in  $X$  and  $Y$  by the step sizes specified, resulting in a diagonal pattern of pointing centers. It results in an optimally homogeneous coverage of the field by the mosaic, for a given number of exposures.

The 'starext' pattern is more complex. It is designed to keep a small area of the field, containing a bright star, off the CCD array in order to reduce reflections. The size of this box area can be specified, recommended values are 8 arcsec  $\times$  8 arcsec. Subject to that constraint this pattern yields the most homogeneous coverage of the field. It works best if the number of exposures is (a multiple of) 5. The move-to-gap acquisition template should be used with this template.

The dither and jitter patterns are illustrated in the Template Manual [RD1].

`OMEGACAM_img_obs_offset` allows full flexibility in the definition of offset patterns. The specified number of exposures are taken, and offsets are taken from a list. Offset data are processed in the same way as `OMEGACAM_img_obs_dither` data. Large offsets beyond the default dither pattern increase the overhead due to the need to reacquire a guide star. See Sect. 3.1.1 and the Template Manual [RD1]. Note that if the template is the last template of an OB, then the return to origin is always skipped.

### 3.4.3 Nighttime Calibration

A number of templates are provided for photometric zero point and atmospheric extinction measurements. Usually, these will be used by Observatory staff executing the calibration plan [RD2], see Sect. 4.1. These OBs need not be specified as part of a science programme.

`OMEGACAM_img_cal_skyflat` takes a sequence of five sky-flats per filter, with typically 2-3 filters that can be observed in evening twilight. The skyflat template will gradually increase the exposure times during a sequence to ensure constant flux level for the five flats, of order 20000-30000 counts. Skyflats are not observed during morning twilight for operational reasons.

`OMEGACAM_img_cal_zp` takes an exposure of a standard field through any filter using the two-lens corrector. Twice per night an equatorial standard field is observed for the five filters  $u'g'r'i'z'$  (see Table 10). The first execution is typically done in the evening twilight, after skyflats. The second execution is done in the middle of the night. Furthermore, when science observations in user bands are done (B, V,  $v$ , Narrow Band filters), an equatorial standard field is also observed in these respective filters.

`OMEGACAM_img_cal_monit` takes an exposure of a polar standard field (see Table 10) through the composite  $u'g'r'i'$  calibration filter, using the two-lens corrector. This is typically done three times per night: end of evening twilight, middle of the night, end of the night.

### 3.4.4 Overheads

There are various overheads associated with OmegaCAM observations. Telescope preset to a new target typically takes about 2 minutes (slew speed better than 1 deg/s). An additional overhead of PA/2 seconds is added for Position Angle (PA) on sky different from 0 in the acquisition. This overhead

Constant	Value (seconds)	Remark
READOUT_TIME	40	Readout + Data written to disk
READOUT_TIME_LAST_IMG	0	Readout for last image of an OB
FILTER_SETUP	65 or 115	Filter exchange between acquisition & 1st science template Depending on filter position, see text.
FILTER_SETUP_TPL	35 or 85	Filter exchange between science templates.
TEL_PRESET	120 + PA/2	2 minutes Preset, plus rotator repositioning
TEL_PRESET_CONCAT	30 + x/1.5	x is distance to new target in degrees
TEL_PRESET_ROT_CONCAT	0-180	For PA != 0 in a concatenation, there is a rotator motion overhead of PA/(1 deg/s)
TEL_OFFSET	15	Telescope offset at the beginning of a science template
INS_GUIDESTAR	60	Total time for GS at the OB beginning.
INS_IASSTAR	180	Time for IA at the OB beginning.
INS_GUIDESTAR_NEW	60	Acquire new GS after offset.
INS_GUIDESTAR_RE	5	Automatically reacquire same guide star after offset.
PICK_TIME	45	Time for pick object for MoveToGap acquisition.

Table 9: The various overhead times associated with OmegaCAM observations.

occurs because to reach any PA angle, the telescope will first preset to the new position at PA=0, and then reposition the rotator, with a speed of about 2 degrees per second. PA < -180 or PA > 180 is interpreted as modulo 360 degrees. For example, PA=270 implies a motion to PA=-90, and hence 45 seconds overhead.

Filter exchange in the instrument is done in parallel to the preset; it takes between 65 and 115 seconds (the precise value depends on whether a filter is being swapped for another one from the same magazine, or whether they belong to different magazines).

Acquisition of guide stars takes about 1 minute. A full IA sequence in the acquisition takes on average 3 minutes. Successive bias frames can be read out every 40 sec, which covers the time needed to wipe the array, read it out and transfer it to disk (ordering the data into a FITS file takes place in parallel to taking the subsequent exposure).

For concatenations an additional overhead applies if a PA different from 0 is chosen in subsequent OBs. In a given concatenation, the amount of this additional overhead equals

$$\text{TEL\_PRESET\_ROT\_CONCAT} = (\text{abs}(PA_{OB<n>}) + \text{abs}(PA_{OB<n+1>})) / \text{Rotatorspeed} \quad (6)$$

Rotator speed is about 2 deg/s. For concatenations where PA is equal for all OBs, the associated overhead per OB is hence the PA angle in seconds. PA=90 would imply an overhead of 90s per OB.

Table 9 collects the currently known overhead values/best estimates. **As of P92**, some overhead reduction is achieved due to parallelising readout and preset/filter-setup. Last readout of an OB is effectively 0 seconds, and filter changes between templates are 30s faster. First offset in a template is now charged with 15s instead of 20s.

#### Some guidelines to avoid unnecessary overheads:

- No guiding is necessary for integration times < 60s. For requested seeing > 1.2'' and zenith distances > 10 degrees, up to ~ 2 minute integrations without guiding are probably fine.
- Concatenate OBs of the same field, if not already contained in a group or time-link container.
- No IA is necessary in the acquisition of concatenated OBs during the first 30 minutes of a concatenation.



- If possible, avoid filter changes within an OB. The overhead for filter change in a preset is zero, since preset and filter exchange are done in parallel and preset takes normally longer than filter exchange. In contrast, filter change between templates costs time: while since P92 this happens in parallel to the readout, it still takes longer than readout and thus adds overhead
- Avoid, if possible, sequences of large offsets beyond the default dither pattern with long integration times. This will require reacquisition of guide stars at each offset. P2 will charge you one minute extra overhead for each large offset, provided that AG is enabled in the acquisition.

### 3.5 Survey Area Definition Tool

To help users in planning how to cover their target survey area a specific tool has been developed, the Survey Area Definition Tool (SADT).<sup>6</sup> It is a mandatory tool for preparing survey observations with the Visible and Infrared Survey Telescope for Astronomy (VISTA), but it may also be used for preparing VST/OmegaCAM survey observations. The output of the SADT (survey area file in XML format) can be used together with the P2 for Surveys to generate automatically large numbers of OBs.

A large survey consists of many 'tiles', or pointing centers. Observations of any type (stare, jitter, dither, offset) can be executed at a tile position. The SADT provides the tiles (and their central coordinates) that may be used to cover any given area of sky. Alternative ways of tiling the sky, e.g. the Astro-WISE 'PlateSystem' developed for the KiDS survey, may also be used but are not supported by the SADT.

### 3.6 Selecting exposure times and number of sub-exposures

ESO provides an Exposure Time Calculator (ETC) for OmegaCAM<sup>7</sup>. It may be used to estimate signal-to-noise, count rates, etc., for OmegaCAM observations.

The sky background varies considerably with filter and with moon phase. The ETC gives the sky count rates per pixel at various moon phases. It is important to make sure that the read noise of the CCDs (5-7 electrons, equivalent to the noise of a 30 electrons per pixel background) does not add significantly to the sky background noise. Exposure times should ideally be such that the sky background is above 250 electrons per pixel. Particularly with the  $u'$  and narrow band filters this requires minimum exposure times of several minutes, particularly in dark time.

### 3.7 Special features of the data

OmegaCAM data, as other wide-field CCD imager data, have several features that complicate data analysis. Data reduction software can cope with these, but it is important to be aware of them.

#### 3.7.1 Point Spread Function

The focal plane of the telescope is not totally flat, such that even with perfect image analysis performed with the OmegaCAM auxiliary chip, mild PSF variations across the field-of-view are unavoidable. This applies both to FWHM and ellipticity, and is in general more pronounced for redder filters. In Fig. 24 we show a PSF anisotropy analysis plot obtained for a 240 seconds i-band exposure. IQ variations of 10-25% across the FOV can occur, depending on outside seeing, filter and telescope mirror position.

<sup>6</sup>For more information about SADT see <http://www.eso.org/sci/observing/phase2/SMGuidelines/SADT.html>.

<sup>7</sup><http://www.eso.org/observing/etc/bin/gen/form?INS.NAME=OMEGACAM+INS.MODE=imaging>

'SF Anisotropy for frames with DATE-OBS 2011-09-03 02:29:07, filter SloanI (32 frame(s)), target=KIDS\_339.0\_-31.  
Alt=62.385 Az=290.349 Rot=96.5557 Seeing=0.92 WindDir=200.0 Winsp=2.69

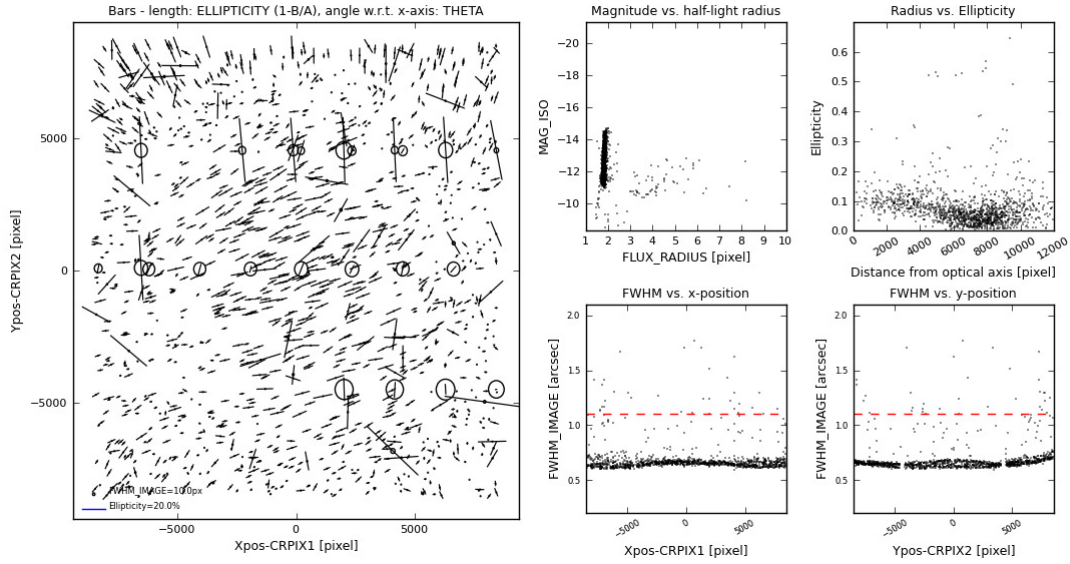
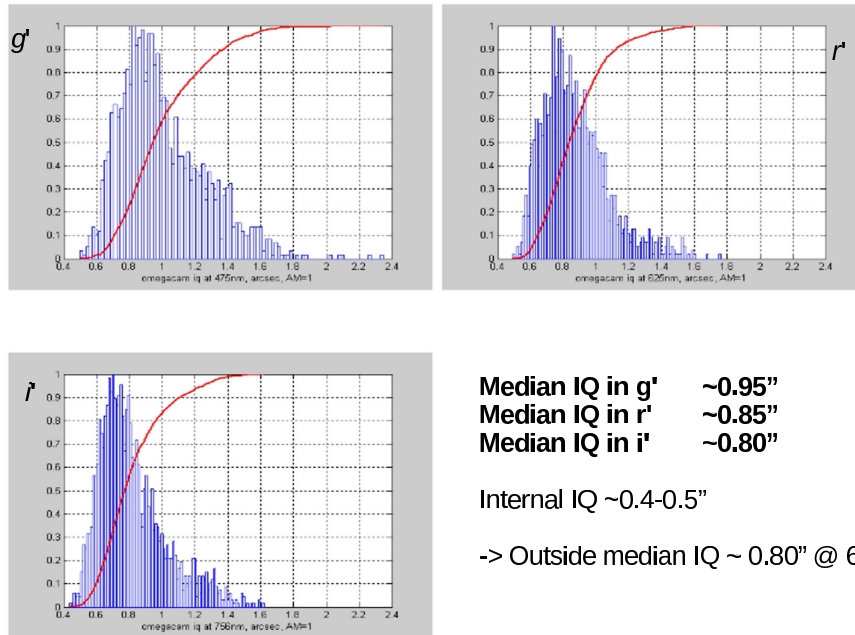


Figure 24: PSF anisotropy analysis plot obtained for an i-band observation. For the given example, outside seeing as indicated by the DIMM (around V-band) was  $0.9''$ , and IQ on OmegaCAM chips was  $\sim 0.65''$ . In general, IQ variations of 10-25% across the FOV can occur, depending on outside seeing, filter and telescope mirror position.

### OmegaCAM IQ distribution August – December 2011

-- each data point is average IQ in one image over full chip array --



© Julio Navarrete, ESO Chile

Figure 25: OmegaCAM IQ distribution, collected between August and December 2011.

Fig. 25 shows a histogram of the PSF FWHM measured in the  $g, r, i$  bands between August and December 2011. Median IQ on the detectors is  $0.8''$  for  $i$ , and  $0.95''$  for  $g$ . Given the internal IQ of  $0.4\text{--}0.5''$ , the measurements are consistent with a median Paranal seeing of  $0.8''$  at 600nm.

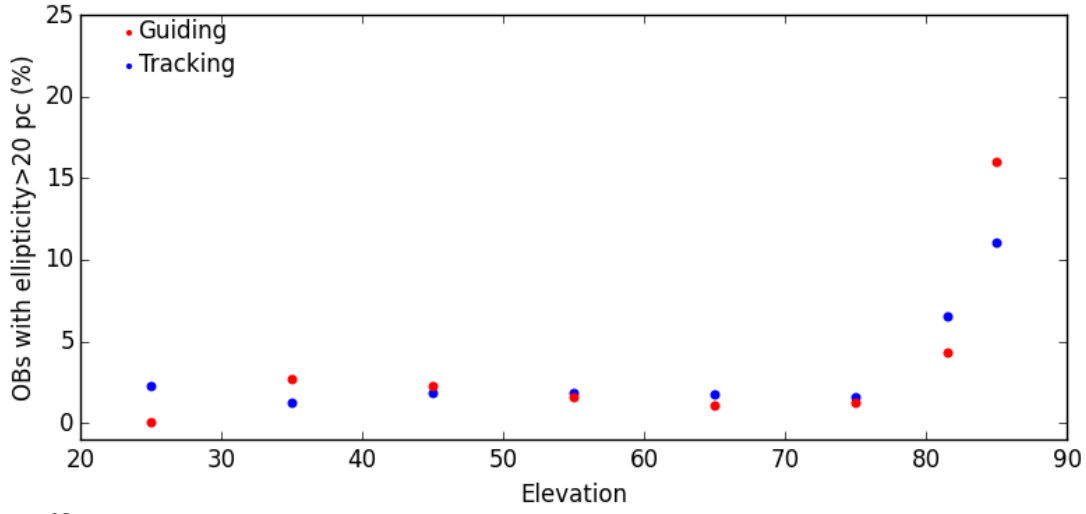


Figure 26: Fraction of OmegaCAM science OBs that show ellipticity of more than 20 percent against telescope elevation. In service mode these observations are normally rescheduled. The range of data is from April 2016 to August 2017.

Fig. 26 shows the percentage of OBs that suffer from more than 20 percent average ellipticity for data taken between April 2016 and August 2017 as a function of telescope elevation. From P101 service mode OBs will normally not be executed when the elevation exceeds 83 degrees. To be confirmed by experience if we continue this policy during P102 and later or revert to the current zenith avoidance distance of 3 degrees.

### 3.7.2 CCD blemishes and particle hits

The OmegaCAM CCDs contain a number of cosmetic defects: hot pixels, cold pixels, and traps (see Table 1). The data on these pixels must be masked out before the data can be analysed; if such gaps in the data are unacceptable the observations need to be dithered, or at least jittered. Hot pixels and traps can result in entire columns of data being lost, so jitter/dither offsets must not be parallel to the CCD columns.

Some dust particles are also visible on the detectors: mostly these cover patches no more than about five pixels (1 arcsec) in size. At this point it is not clear whether/how often the dust particles move around.

In addition, particle hits on the CCDs release charge and obliterate small parts of the image. If these are a concern (their number grows with the exposure time) then several exposures are needed.

### 3.7.3 Ghosts and reflections

Unwanted (but at some level unavoidable) reflections at air/glass and air/silicon interfaces result in some scattered light in the image. Some of these reflections are reasonably well-focused, resulting in ‘ghost’ reflections — spurious images from bright sources, appearing in different parts of the field. In OmegaCAM most of these ghosts are very defocused and hence very diffuse, but the most focused one projects to radii of a few mm (scale is  $14.3''/\text{mm}$ ) and so is visible if there is a bright star in the

field. It arises as a reflection off the entrance surface of the dewar window, followed by a reflection off the nearest filter surface. Another ghost arises as a reflection off the CCDs, followed by reflection at the entrance or exit surfaces of the dewar window. (These reflections largely disappear when the star falls on a gap between CCDs.)

By way of example, Fig. 27 shows the four main reflections from a bright star on CCD #91. The associated table lists typical size and surface brightness (relative to the bright star) of these ghosts. Note that the sizes and positions of the ghosts depend on the location of the parent star in the image, and their brightnesses on the filter in use.

Ray tracing calculations predict that a bright star at distance  $R^\circ$  degrees from the center of the field will have a ghost that is displaced radially outwards by

$$21'' R^\circ + 70'' R^{\circ 3} \quad (7)$$

and that this ghost has a diameter of

$$23'' + 73'' R^{\circ 2}. \quad (8)$$

In some cases, reflections from stars outside the field are seen. Their origin is still under investigation. Initial results are that these are caused by bright stars which lie between 0.5 and 0.53 degrees E or W (in the default orientation of the mosaic) of the pointing center, in the top or bottom row of CCDs. The reflections are linear, narrow features perpendicular to the edge of the mosaic. An example is shown in Fig. 28.

Stars outside the top and bottom edges also cause linear reflections, but less frequently. They require a star 0.56–0.565 degrees N or S of the pointing center. These reflections are weaker and less focussed than the previous ones. Their cause is also still under investigation.

### 3.7.4 Sky concentration

Multiple reflections also generate a very defocused image of the field, which is added to the sky background in the image. The effect, usually referred to as ‘sky concentration’, is a smooth, additive component to each image.

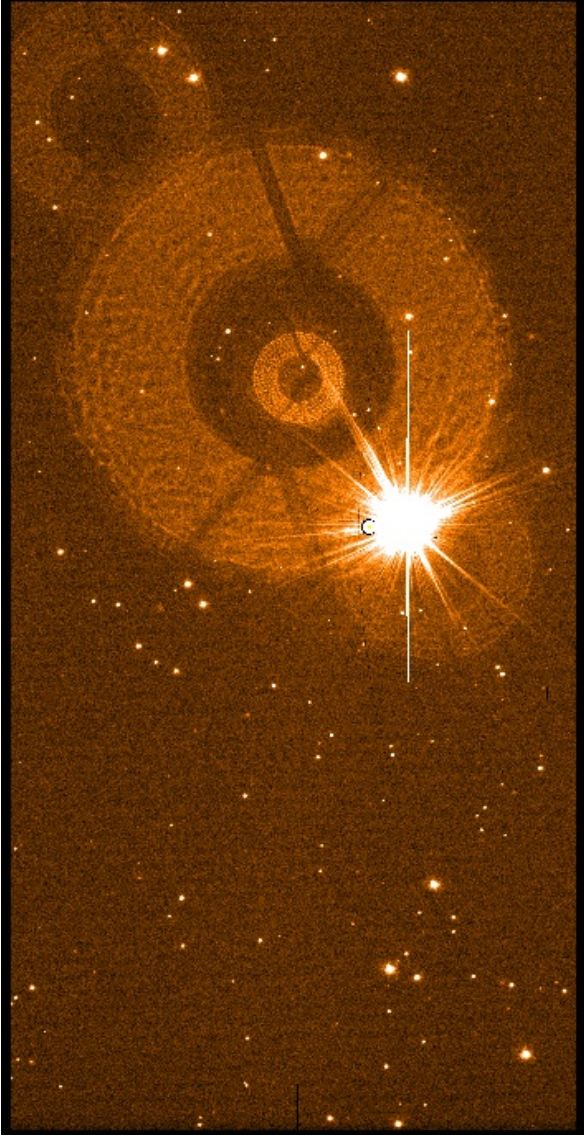
The additive term is also present in flat fields, be it from the sky or from an exposure of the dome screen. If this additive term is not subtracted from the flat fields first, the result of flat-fielding is an image with a flat background but a varying photometric zero point.

Determining such a ‘photometric flat field’ is best done by observing large standard star fields. Note that one way to mitigate the effect is to calibrate each exposure CCD by CCD, since the pattern is expected to be dominated by scales larger than an individual chip.

Sky concentration has been shown in commissioning to be for Sloan band observations up to 20% in twilight and ~5% or less in dome flats. See also Sect. 2.9.

### 3.7.5 Vignetting close to wind mast position

Test sky flats taken in November 2012 showed that the VST pupil is vignetted by several percent by the Paranal wind mast, when the telescope points at altitude  $<45$  degrees and  $162 \pm 5$  degrees azimuth. This is in the north-north-west. Fig. 29 shows the respective sequence of sky flats taken at 40 degrees altitude and  $\pm 5$  degrees from the mast. The linear structures are from the wind mast.



Ghost	radius (arcsec)	surf.br. $\Delta\text{mag}/\text{arcsec}^2$	remark
1	70	16	window/filter
2	330	16.6	CCD/outer window
3	150	17.1	CCD/inner window
4	160	17.6	window/filter

Figure 27: Example ghost reflection from a  $g' = 6.5$  magnitude star in a 60-second  $g'$  band exposure, in CCD #91. The ghosts line up along a radius vector through the center of the array, which is towards the bottom right in this case. Appearances will be different in other locations. Ghosts are numbered in order of decreasing surface brightness: from top bottom, numbers 4,2,1,3. The table on the right gives their radii and surface brightness, scaled to a magnitude zero parent star. If stars of this brightness or above as well as OmegaCAM observations were uniformly distributed in the sky, every fourth to fifth field would contain one such star.





Figure 28: Example of reflection of light from a star (in this case, two stars to the West) outside the field. Such features can occur on each of the four corner CCDs.

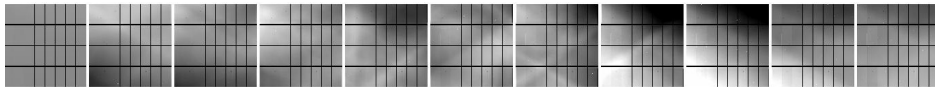


Figure 29: Vignetting of the VST FOV by the Paranal wind mast - Each image shows a normalised sky flat taken at a telescope altitude of 40 degrees, and at azimuth angles between 157 and 167 degrees (from left to right). Normalisation is done wrt the mean of the leftmost and rightmost image. Greyscale is from  $\pm 10\%$  of the mean flux. The sequence crosses the position of the Paranal wind mast at around 162 degrees azimuth (north-north-west). Amplitude of the linear structures caused by the wind mast is several percent.

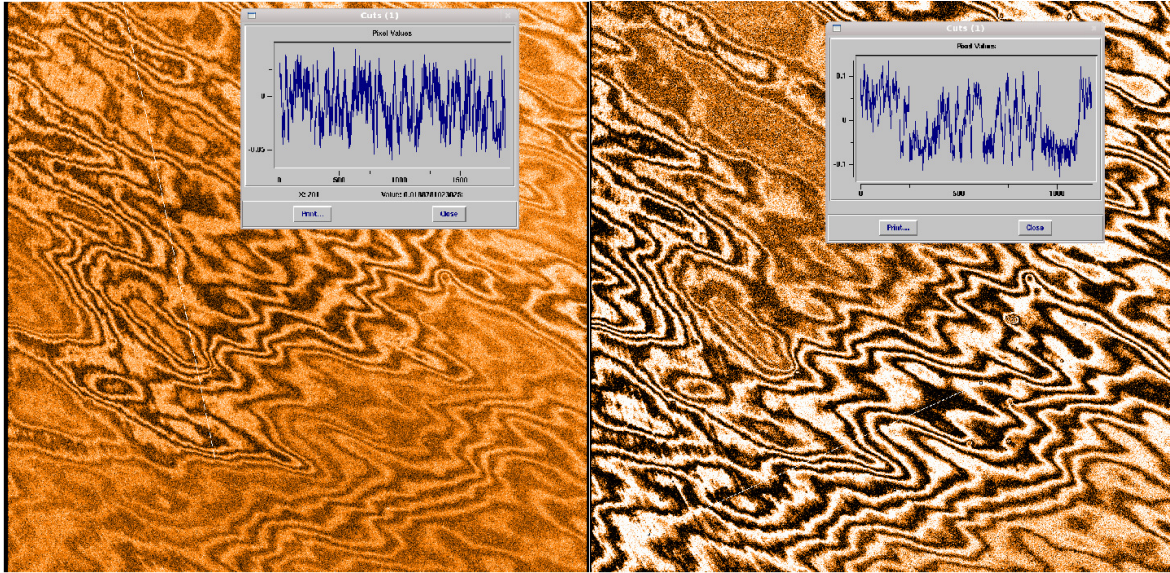


Figure 30: excerpts of a fringe map for the Sloan  $i'$  (left) and  $z'$  band (right). Intensity contrasts in the image are at  $\pm 5\%$ . The cuts show that fringe amplitudes are a few percent in  $i'$ , and up to 10% in  $z'$ .

### 3.7.6 Diffraction Spikes

The spider that holds the secondary mirror in place causes diffraction spikes around bright stars. Because the VST is an alt-az telescope, the camera rotates with respect to the spider during an exposure, causing this spike pattern to rotate as well.

### 3.7.7 Fringes

Internal reflections in the CCD and the consequent interference give rise to fringes in the sky background. These effects show up in the  $i'$  and  $z'$  bands (and to a low extent in  $r'$ ), and can have amplitudes up to  $\sim 10\%$  in  $z'$  band. The fringes are caused by the emission lines in the night sky spectrum, and can be highly time-variable. As the equivalent width of these lines varies in the sky spectrum so do the fringe amplitudes and to some extent the patterns. This additive effect is mapped by comparing twilight sky exposures (with relatively weak sky emission lines) with dark sky exposures. Appropriately scaling this ‘fringe map’ to individual exposures then allows the fringe pattern to be subtracted.

Fig. 30 shows excerpts of a fringe map for the Sloan  $i'$  and  $z'$  bands, with intensity contrasts in the image at  $\pm 5\%$ .

### 3.7.8 Remanence

Exposure to a very bright star can saturate the CCD, and can leave a surplus of charge on the surface of the detector. This can take some time to diffuse away, and meanwhile any subsequent readouts will show a faint residual of the saturated star. Such remanence can take well over half an hour to decay away. Note that remanence on your service mode data may indeed be caused by a previous image obtained for a different program. Overall, if naked-eye stars as well as OmegaCAM observations were uniformly distributed in the sky, every fourth to fifth field would contain one such star that could leave notable remanence.

### 3.7.9 CCD Crosstalk

CCDs # 93-96 are known to suffer some electronic crosstalk. Since crosstalk has not been found down to very low levels in any of the other CCDs, the explanation lies either in the CCDs concerned themselves or some manufacturing problem of the detector-head electronics. There are no current plans to take remedial action as any intervention in the detector head entails a high risk.

The crosstalk has its origin in bright objects. The threshold for triggering crosstalk depends on the CCD and exposure time. Mostly it requires saturating the A/D converter, but also unsaturated sources can lead to electronic ghosts in other CCDs, at a level of up to 0.4% of their 'parent'. These ghosts look like real sources and cannot be removed by dithering.

The crosstalk can be both positive (bright) and negative (dark) with a range of up to 0.4%; it is generally weaker the larger the distance between source and target CCD is. The ghost images always occur at the same relative pixel coordinates in the target CCD, at which the star in the source CCD is located.

The crosstalk pattern present in any image consists of several sub-patterns (see Fig. 31). The most common ones are:

(i) Negative crosstalk from #96 to #95. This is always present. (ii) Positive crosstalk from #94 to #95 and on to #96. It seems that #95 may sometimes be skipped over. (iii) Positive crosstalk from #96 to #95 to #94 and, very rarely, to #93.

The OmegaCAM consortium is working on dedicated data reduction procedures to flag or remove these artefacts.

The effect of this crosstalk on the flat fields is still to be investigated in detail.



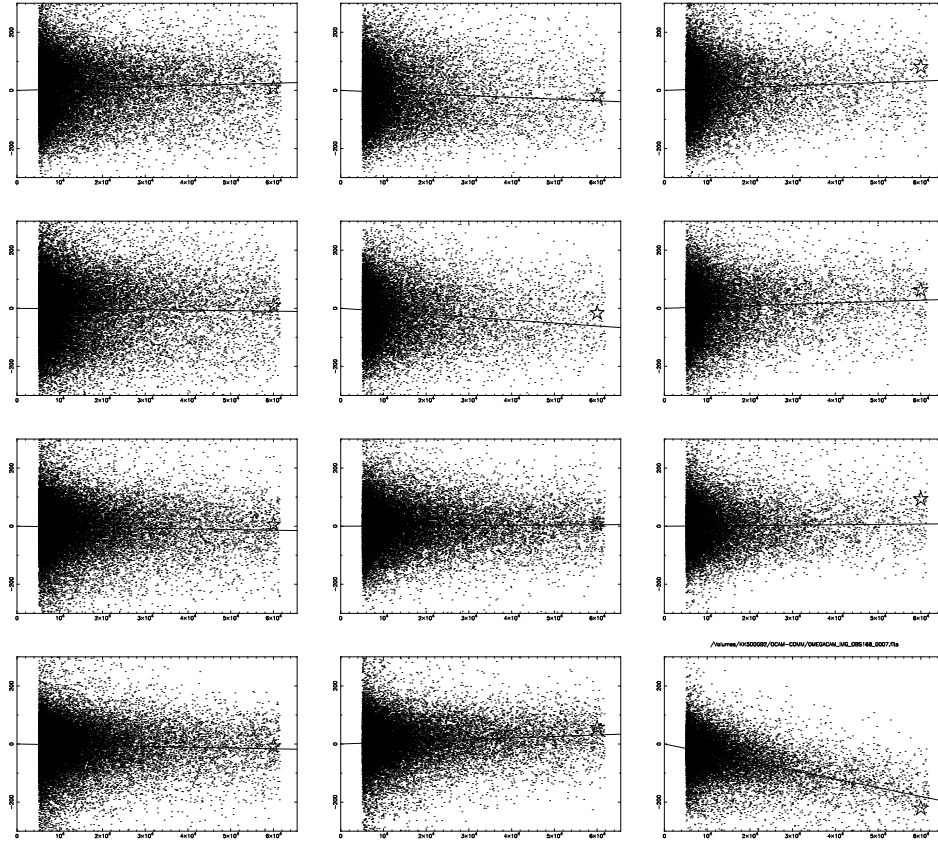


Figure 31: Crosstalk between CCDs \$93–96. Each panel shows the counts in a 'receiver' CCD as a function of the counts in another 'emitter' CCD. Positive/negative slopes correspond to positive/negative crosstalk. In several cases there is a clear linear relation, illustrating crosstalk from unsaturated pixels. Saturated pixels also cause crosstalk in many combinations of emitting and receiving CCD: their median count level is shown as a star. Each row corresponds to a different receiver CCD; within a row the three possible emitter CCDs are plotted in numerical order.

## 4 Calibrating and Reducing OmegaCAM data

All OmegaCAM data are taken in service mode, in the context of a calibration plan [RD2] whose function is to maintain the overall calibration of the instrument and atmosphere. Thus the aim is not to calibrate individual data sets, but rather to calibrate the sky+telescope+instrument chain.

Data volumes from OmegaCAM are LARGE. A single exposure leads to 0.5 GB of raw uncompressed data (at 2 bytes per pixel); processed exposures, with a 4-byte real number per pixel, are over a gigabyte in size. Typical data volumes from a single night are 50-100 GB of raw science data; another 20-50 GB of raw calibration data are also taken every day.

OmegaCAM data are processed using a pipeline (see [RD3] for a full description) which is run by the ESO Data Flow Operations group, and is used for quality control purposes [RD7]. On Paranal, a special version of the pipeline is running for real time QC0 checks of image quality (FWHM, ellipticity, IQ variation) and sky transparency. Only raw data is made available to the general user.

All data from OmegaCAM are delivered as multi-extension FITS files. The first extension contains the observing parameters, and extensions 2-33 contain the data from the individual CCDs. Note that the name of the CCD, as identified in Fig. 3 is included in the header of the corresponding FITS extension. The order in which extensions appear in the FITS file may vary and should *not* be relied upon to identify CCDs.

### 4.1 Calibration Plan

The full details of the original calibration plan are given in a separate document [RD2]. We summarise the important features of its Paranal implementation here, noting that all calibrations mentioned in the following are 'free of charge' for the user.

Bias, dark and flat field exposures are taken regularly on a daily to weekly basis. Biases are taken daily, dome flats every 3-5 days, and darks weekly. Note that occasional jumps in the bias levels occur, attempts to eliminate these jumps are continuing. See:

[http://www.eso.org/observing/dfo/quality/OMEGACAM/reports/HEALTH/trend\\_report\\_BIAS\\_level\\_HC.html](http://www.eso.org/observing/dfo/quality/OMEGACAM/reports/HEALTH/trend_report_BIAS_level_HC.html)

In clear conditions, sky flats are taken every night in 2-3 filters. One can hence expect each key band to have sky flat every 3 days. Master flat fields are derived from a combination of twilight and dome flats (but note the impact of straylight gradients in sky flats, Sect. 2.9). Fringe maps are derived by comparing these flat fields to night-sky exposures.

The photometric zero point is determined as follows. The basic approach is that the atmospheric transparency and instrument efficiency are monitored several times per night in the five SDSS bands ( $u'g'r'i'z'$ , the so-called *key bands*) using the two-lens corrector, whereas other filters (so-called *user bands*) are cross-calibrated against these. All filters, including  $u'g'r'i'z'$ , are considered as *user bands* when they are used in combination with the Atmospheric Dispersion Corrector (ADC). The ADC is not offered and will be removed from templates in P99.

OmegaCAM employs a 4-quadrant calibration filter, which is used to monitor the sky transparency and the instrument zero point in  $u'g'r'i'$  bands simultaneously. Three times a night, a standard star field on the celestial pole is observed with this filter to measure atmospheric extinction. In evening twilight and around midnight, and for clear conditions, a high-elevation Landolt standard star field is also observed in the five bands  $u'g'r'i'z'$  (see Table 10), with the monolithic science filters from the SDSS system. Finally, if science observations in user bands are made, an equatorial standard for the those particular bands is also observed close in time to the science observation.

When telescope pointing restrictions due to wind apply, it may not be possible to observe any Landolt equatorial standard star field during an entire night. In this case, backup standard fields in the

## Monitoring the Photometric Calibration

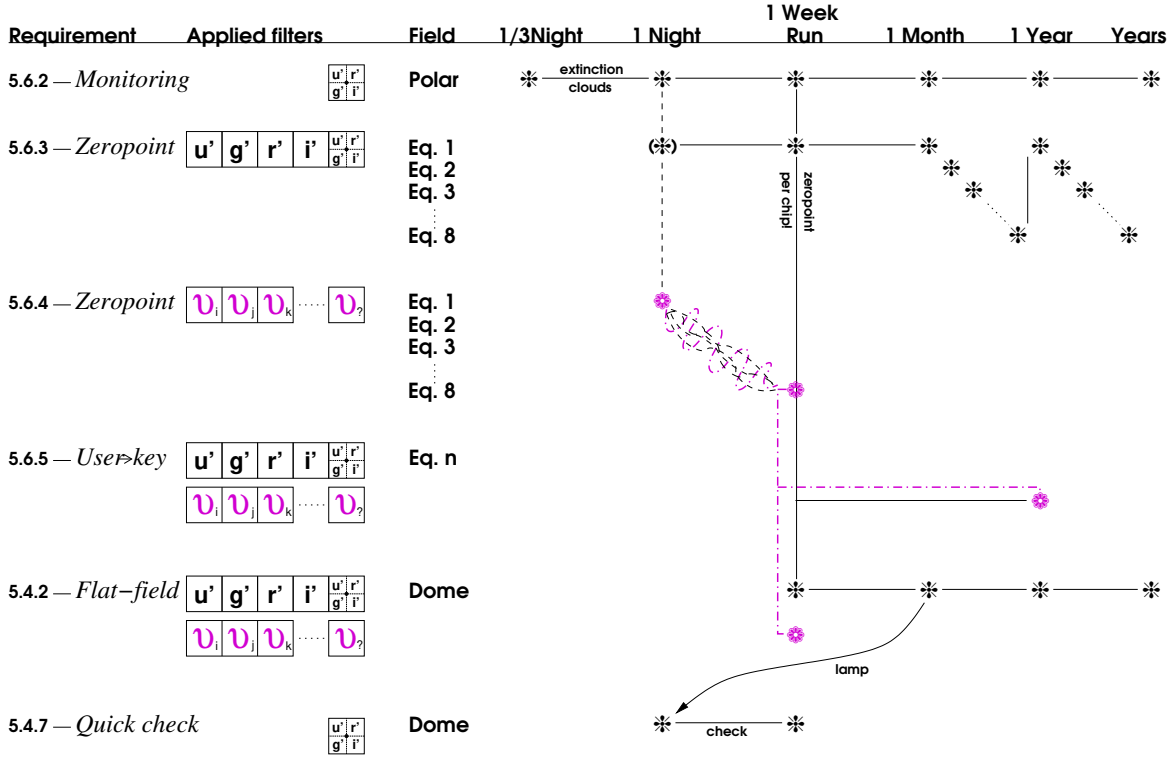


Figure 32: The frequency with which the various types of calibration data are taken. More details are given in the Calibration Plan [RD2]. The symbol  $\mathcal{U}$  denotes a user band.

southern hemisphere are observed, taken from the Stetson catalog.<sup>8</sup>

Figure 32 shows schematically with what frequencies calibration data are typically taken. During the first year of operations, regular observations of extended Landolt fields are taken to provide a comprehensive set of secondary standards for the OmegaCAM filter system.

Astrometric calibration is performed by reference to the many USNO catalogue<sup>9</sup> stars that are present on each CCD. No special calibration observations are needed. With the broadband  $g'r'i'z'$  filters and exposure times between 10 seconds and 10 minutes the USNO stars should be unsaturated. Short  $u'$  band observations (less than a minute) may not provide sufficient stars for an accurate astrometric solution.

More specialised calibration files, related e.g. to sky concentration, or fringing from night-sky lines, are derived from the observations themselves, or from less frequent dedicated measurements.

The calibration plan is specified to deliver photometric zero points accurate to 0.05 magnitudes, and astrometry with rms error 0.1 arcsec, in a fully automatic pipeline reduction mode.

### 4.1.1 Calibration of HALPHA and NB659 data

In principle, the pipeline should be able to calculate the HALPHA and NB659 zero points providing that it finds reference standard stars in the catalog. If these do not exist then the following approach

<sup>8</sup><http://www3.cadc-ccda.hia-ihp.nrc-cnrc.gc.ca/community/STETSON/standards/>

<sup>9</sup>The USNO astrometric star catalogues contain over 400 million stars over the whole sky (an average of 10,000 per square degree, or 300 per OmegaCAM CCD), down to  $\sim 20$ th magnitude in  $R$ . Typical astrometric uncertainty for each star is 0.3'' rms. More information on the catalogue can be found at <http://archive.eso.org/skycat/usno.html>.

Field Name	RA	DEC
SA92	00:55:12.0	00:55:58.0
SA95	03:53:49.0	00:02:33.0
SA98	06:52:12.0	-00:19:17.0
SA101	09:56:19.0	-00:26:27.0
SA104	12:42:12.0	-00:30:16.0
SA107	15:39:03.0	-00:13:52.0
SA110	18:41:50.0	00:23:09.0
SA113	21:41:54.0	00:29:22.0
Polar Field	03:25:43.0	-89:02:33.0

Table 10: OmegaCAM Photometric Standard Star Fields

could be tried, i.e. applying ZP offsets with respect to the ZP in R band. The magnitudes are based on the SloanR band with:

$$\text{HALPHA} = \text{SloanR} + \text{OFFSET\_H\_ALPHA}$$

$$\text{HALPHA\_err} = \text{SloanR\_err} \times \text{OFFSET\_HALPHA\_ERR}$$

$$\text{NB659} = \text{SloanR} + \text{OFFSET\_NB659}$$

$$\text{NB659err} = \text{SloanRerr} \times \text{OFFSET\_NB659\_ERR}$$

with

$$\text{OFFSET\_HALPHA} = 2.81$$

$$\text{OFFSET\_HALPHA\_ERR} = 1.0$$

$$\text{OFFSET\_NB659} = 2.81$$

$$\text{OFFSET\_NB659\_ERR} = 1.0$$

## 4.2 Data reduction Pipeline

Data delivered to the ESO archive consist of the raw exposures, as well as the calibration data. The header of the image contains the nominal astrometric world coordinates; they are not corrected for pointing errors, etc. The photometric zeropoint is provided as a separate calibration file.

The OmegaCAM pipeline performs the following main steps, using calibration files derived by the ESO Data Flow Operations Group in Garching:

1. Each CCD frame is debiased
2. Bad pixels are flagged
3. Cosmic rays and satellite tracks are detected and flagged.
4. Data are divided by a normalised flat field image
5. If appropriate, fringes are removed
6. An astrometric solution is computed for each CCD based on a search of USNO stars in the image
7. Images are background-subtracted, corrected for sky concentration and resampled to a common, linear world coordinate system.

8. Different exposures in the same template are combined into one single image per CCD, taking into account weights and bad pixel masks.

It must be stressed that ESO does not provide any reduced science images. Furthermore, and like for VIRCAM, the ESO version of the pipeline is mainly designed for reduction of calibration frames, and it is not released to outsider users. The user should contact the consortium for the pipeline / science grade products.

An alternative available to all "normal" users is that OmegaCAM data can also be reduced by the CASU-pipeline. Users who are PI of an accepted OmegaCAM run must grant access to the data under that program ID before the start of the observing period. This is done by delegating the access to the data to casuhelp@ast.cam.ac.uk via the ESO user portal.

### 4.3 Quality Control

ESO performs real time quality control during the observations, using QC parameters derived by the data reduction pipeline. The main parameters used in real time QC (named QC0 on Paranal) are FWHM, ellipticity of point sources in the science images, and photometric ZPs derived from standard star exposures. For each exposure, and a representative subset of 8 of the 32 CCDs, the above QC parameters are provided as pipeline output and queried with scripts by the nighttime operators. Image Quality average is contrasted with the user requirements to determine whether an executed OB is within constraints. Accepted tolerance is 10% in average FWHM wrt user requirements. Also, ellipticity and image quality variation across the FOV are monitored. OBs whose images have more than 0.15 average ellipticity, or more than 25-30% in FWHM variation across the FOV, are typically rescheduled.

All OmegaCAM data are transferred to Garching via USB disks. In the medium term future it is envisaged to transport the data via a fiber link between Paranal and Antofagasta (EVALSO) to Europe, such that the delay will only be a few hours at most. Health checks of the calibration data are performed by the Quality Control Group in Garching to monitor the status of the instrument [RD 7]. A scoring scheme is applied to those QC parameters. Also the Paranal pipeline provides health check parameters which can be scored to monitor the instrument status. Since November 2011, **no** scientific data are analysed by Quality Control in Garching anymore.

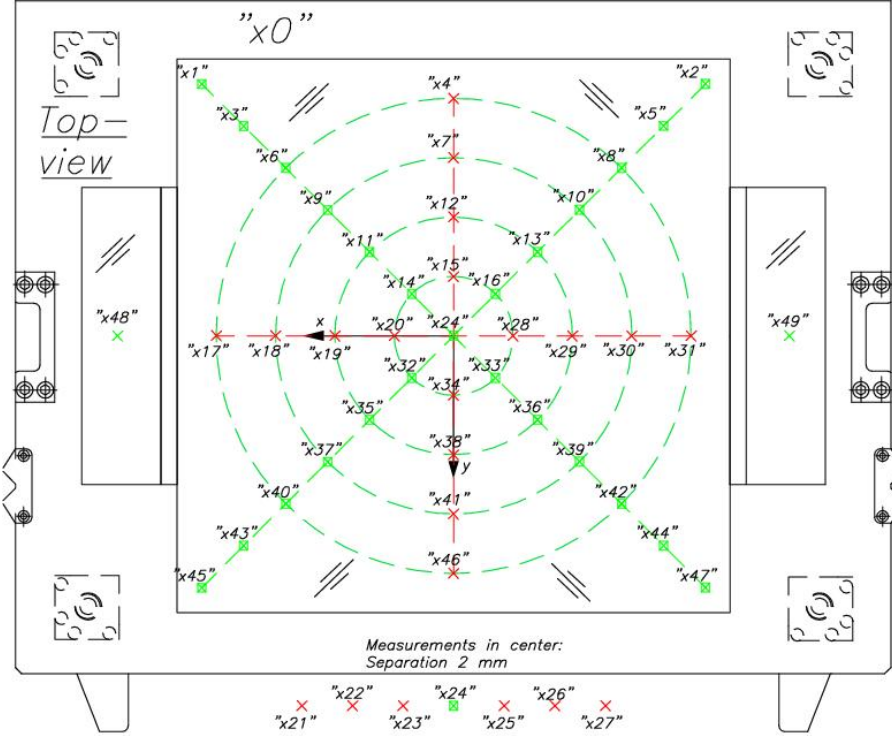


Figure 33: Location of the filter throughput measurements and coordinate system definition. The concentric circles have radii of 29, 57.5, 86, and 115mm; additional measurements on the diagonals were made at radii of 144 and 172mm. The scale on the sky is 14.3"/mm. The  $x$  and  $y$  coordinate axes are indicated; the filter moves towards its positive  $y$  (with the two notches ahead) when it is inserted in the instrument. The filter coordinate system is identical with the instrument coordinate system if the filter is loaded from magazine B.

## A Filter throughput curves

In this section we present the results of measurements of the filter throughput, performed in the lab at the Universitäts-Sternwarte München.

### A.1 Broad band Sloan filters ( $u'g'r'i'z'$ )

As described in Sect. 2.3, the Sloan filters are interference filter sandwiches. Because of the manufacturing process, and because the beam of the telescope crosses the filters under different angles in different parts of the image (see Fig. 2), the bandpass of the filter is slightly field dependent. The laboratory measurements were designed to mimic the converging, tilted beam from the telescope as a function of position in the focal plane.

Below we provide fitting formulae for the radial variation of central wavelength, blue edge and red edge of each filter, as well as plots of the filter profile at the center of the filter. Apart from the wavelength shift, the shape of the filter response is rather constant with field position. *The filter response curves have all been multiplied by the average quantum efficiency of the OmegaCAM CCDs.*

In the case of two filters ( $i'$  and  $r'$ ), the bandpass variation is not quite axisymmetric about the physical centre of the filter. For these a best-fit center was determined; the location of the center is reported in Sect. A.4.

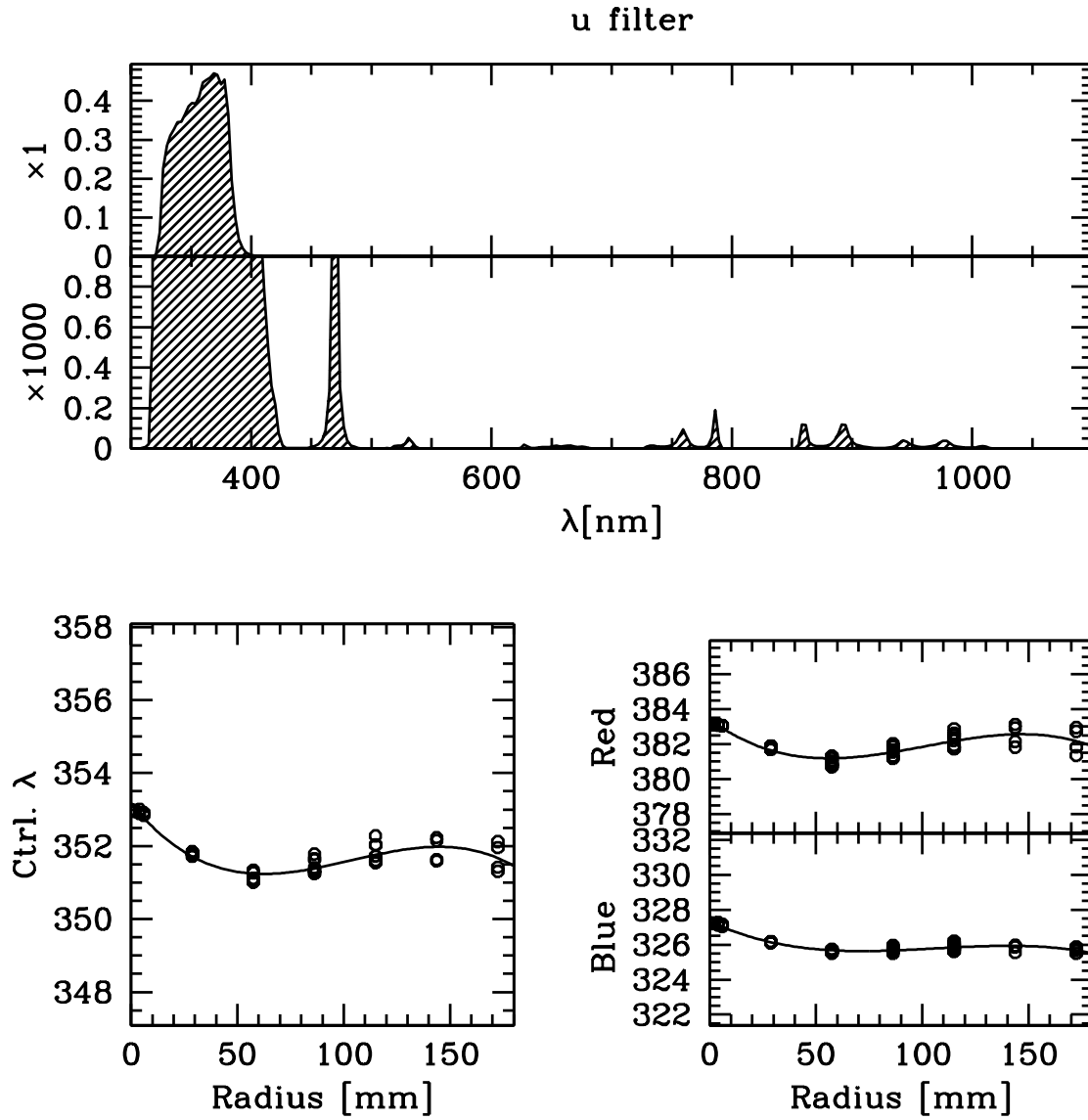


Figure 34: Top panels: throughput of the  $u'$  filter  $\times$  average CCD response curve, including a blow-up by a factor of 1000 to show the out-of-band blocking. Bottom left: variation of central wavelength with radius on the focal plane (dots: measurements; line: polynomial fit). Bottom right: corresponding variation of wavelength at half-maximum throughput of the blue and red edges of the filters. The edge of the CCD array is reached at a radius of  $\sim 180$  mm.

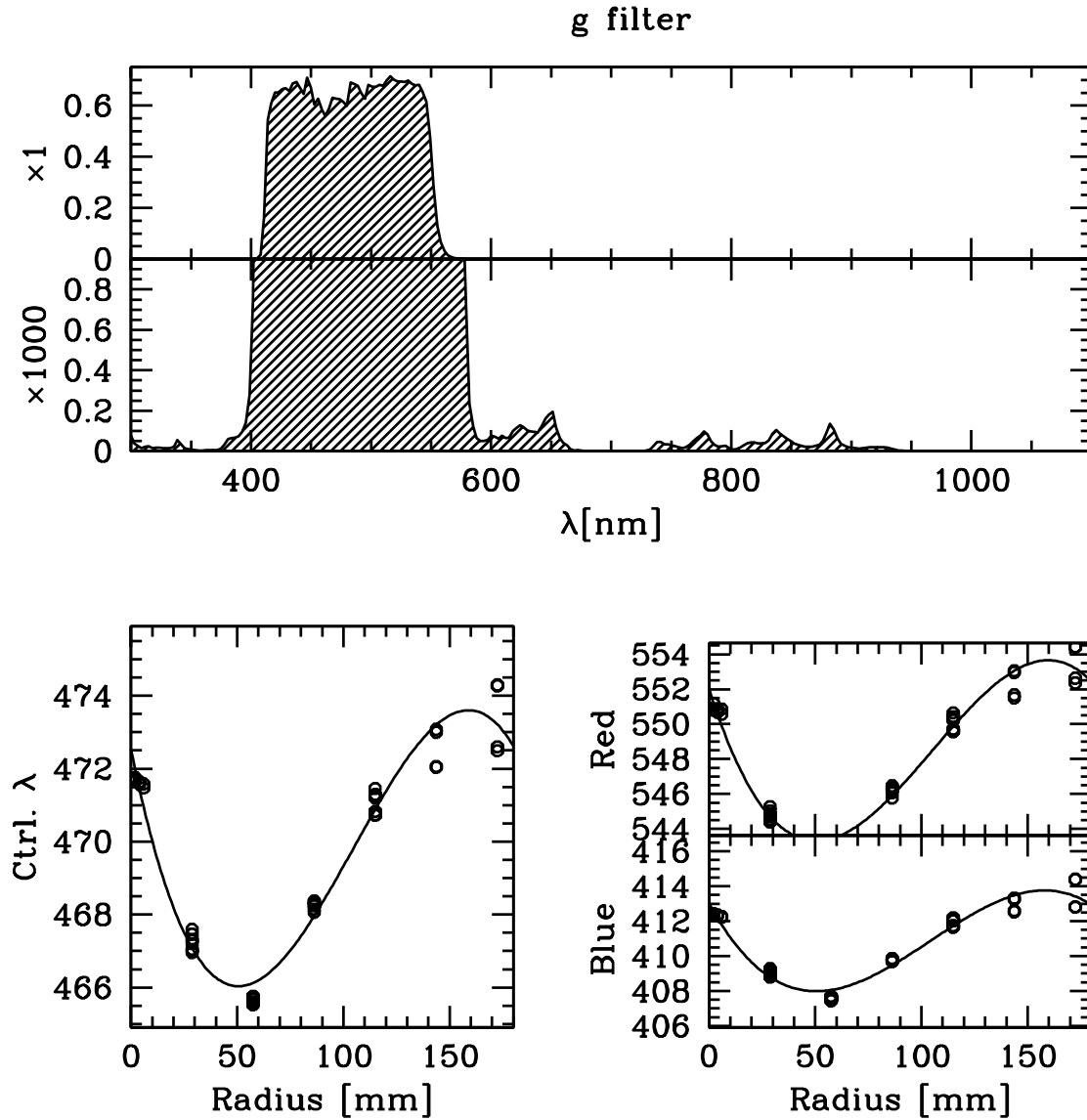


Figure 35: Top panels: throughput of the  $g'$  filter  $\times$  average CCD response curve, including a blow-up by a factor of 1000 to show the out-of-band blocking. Bottom left: variation of central wavelength with radius on the focal plane (dots: measurements; line: polynomial fit). Bottom right: corresponding variation of wavelength at half-maximum throughput of the blue and red edges of the filters.



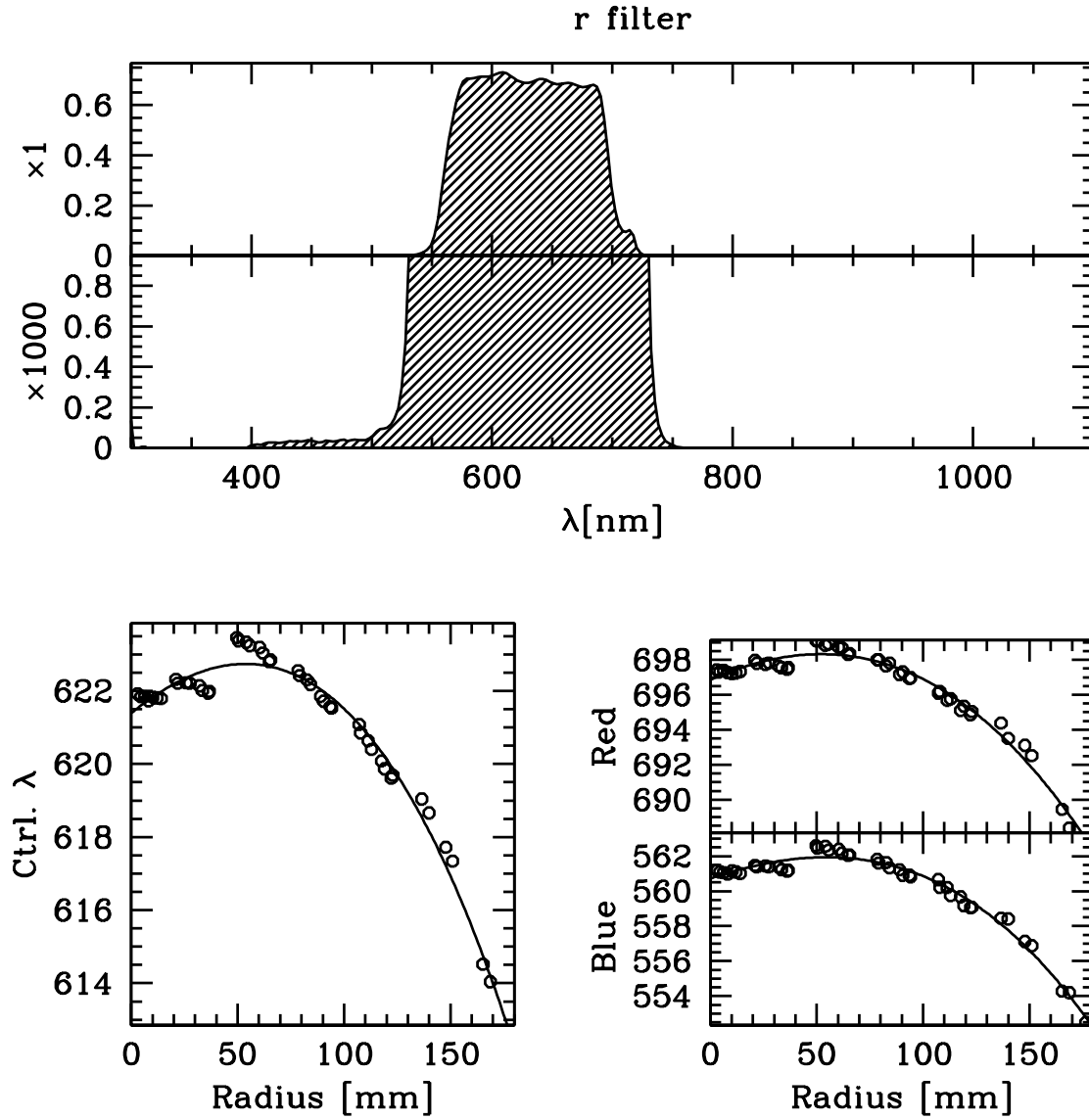


Figure 36: Top panels: throughput of the  $r'$  filter  $\times$  average CCD response curve, including a blow-up by a factor of 1000 to show the out-of-band blocking. Bottom left: variation of central wavelength with radius on the focal plane (dots: measurements; line: polynomial fit). Bottom right: corresponding variation of wavelength at half-maximum throughput of the blue and red edges of the filters. Note that for this filter the bandpass variation is most symmetric about the an offset center—see Sect. A.4.

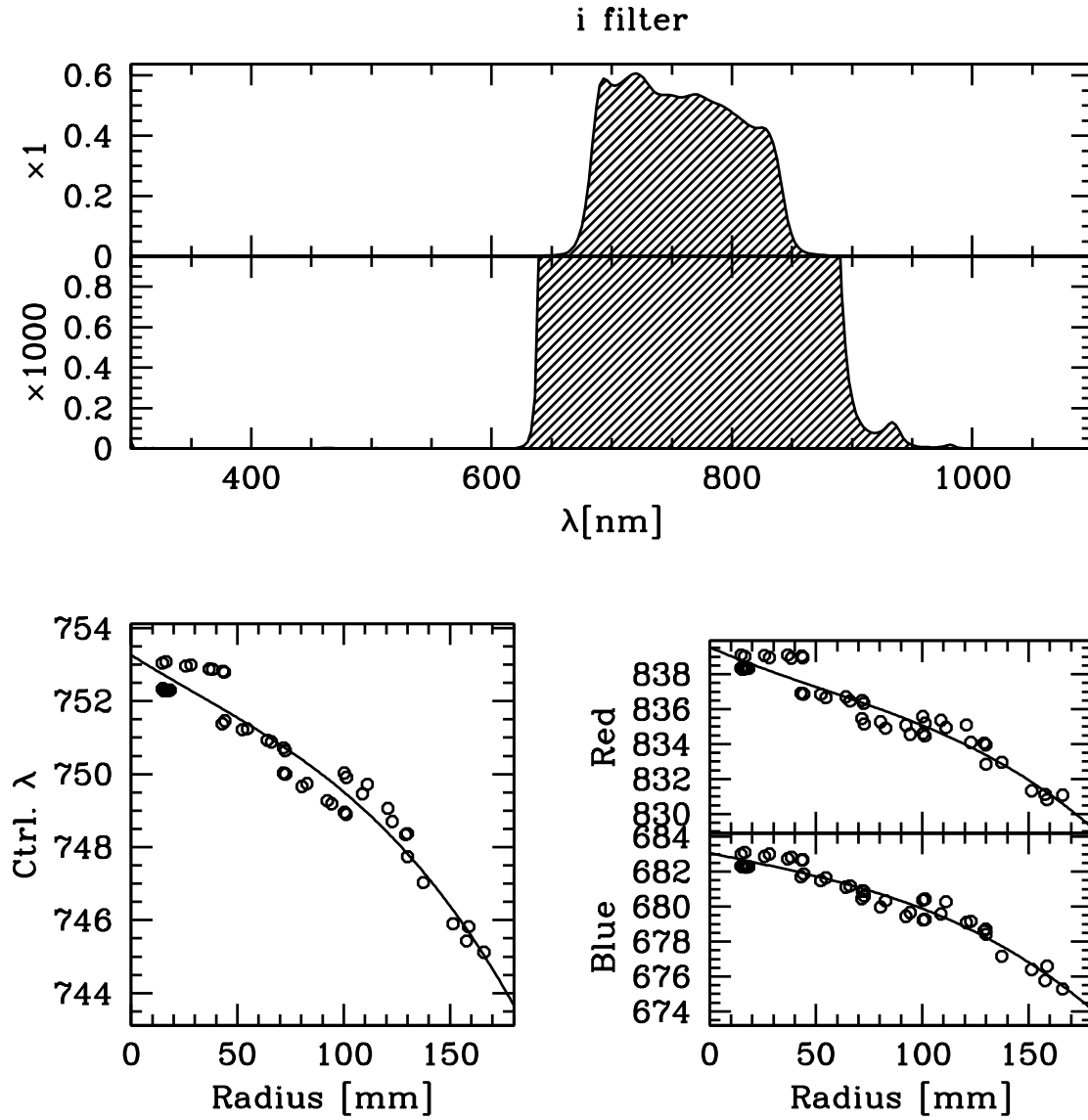


Figure 37: Top panels: throughput of the  $i'$  filter  $\times$  average CCD response curve, including a blow-up by a factor of 1000 to show the out-of-band blocking. Bottom left: variation of central wavelength with radius on the focal plane (dots: measurements; line: polynomial fit). Bottom right: corresponding variation of wavelength at half-maximum throughput of the blue and red edges of the filters. Note that for this filter the bandpass variation is most symmetric about the an offset center—see Sect. A.4.

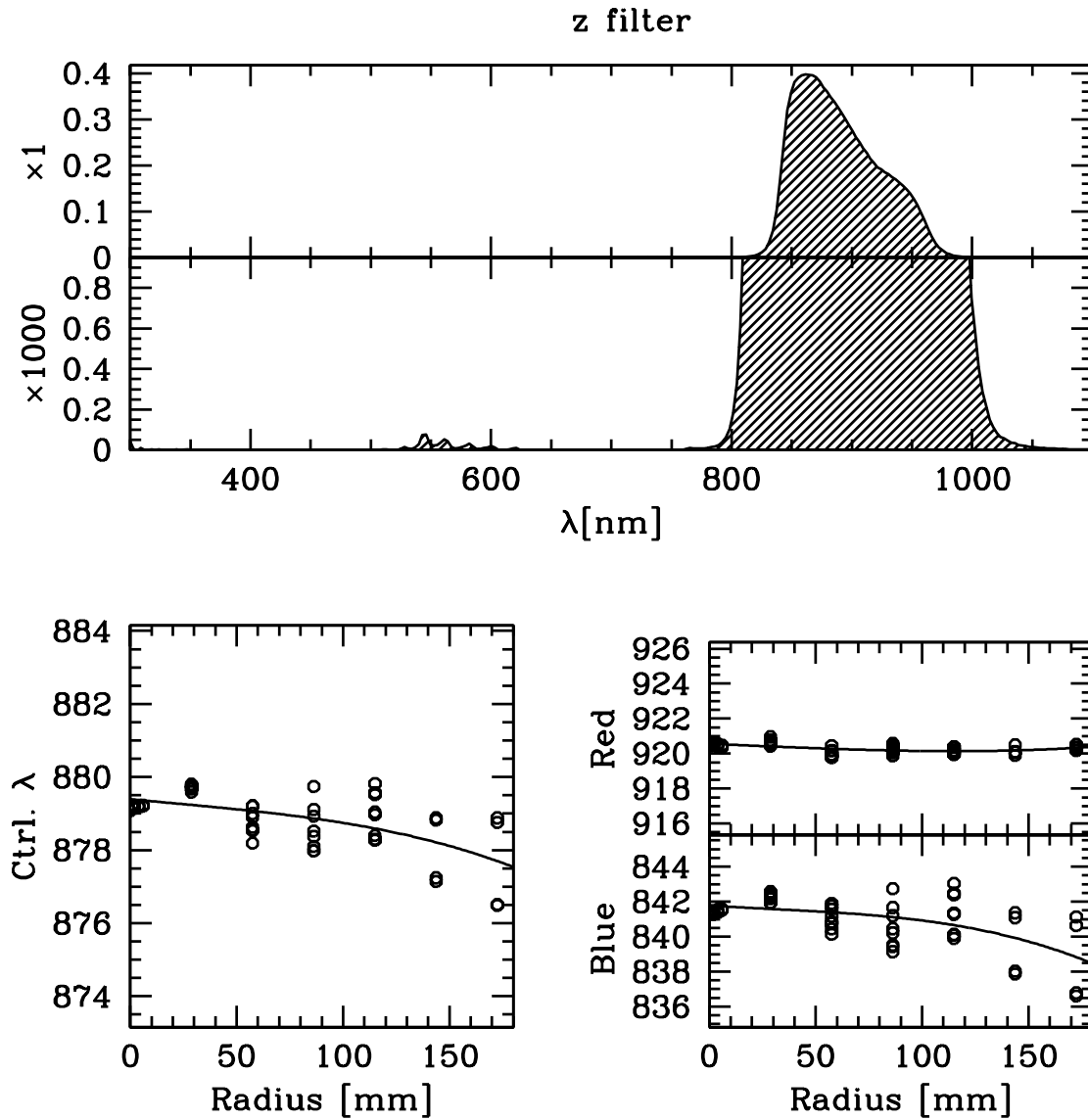


Figure 38: Top panels: throughput of the  $z'$  filter  $\times$  average CCD response curve, including a blow-up by a factor of 1000 to show the out-of-band blocking. Bottom left: variation of central wavelength with radius on the focal plane (dots: measurements; line: polynomial fit). Bottom right: corresponding variation of wavelength at half-maximum throughput of the blue and red edges of the filters.

## A.2 Segmented Broad-band filters (Johnson B and V)

See transmission curve data available from the 'Tools' Section of the OmegaCAM webpage [RD6].

## A.3 Narrow-band filters (Strömgren $v$ and $H\alpha$ )

See transmission curve data available from the 'Tools' Section of the OmegaCAM webpage [RD6].

## A.4 Radial variations in bandpass

The radial variation of central and half-power wavelengths, expressed in nm, can be described as the sum of the following polynomial terms in  $r$  [mm]:

$\mathbf{u'}$		$\times 10^{-2}r$	$\times 10^{-4}r^2$	$\times 10^{-6}r^3$
Central	353.2	-7.24	8.29	-2.66
Blue edge	327.3	-5.71	6.01	-1.89
Red edge	383.4	-9.15	11.27	-3.70

$\mathbf{g'}$		$\times 10^{-2}r$	$\times 10^{-4}r^2$	$\times 10^{-6}r^3$
Central	472.5	-28.72	37.43	-11.91
Blue edge	413.0	-22.29	29.10	-9.30
Red edge	552.0	-38.51	50.15	-15.90

$\mathbf{r'}$		$\times 10^{-2}r$	$\times 10^{-4}r^2$	$\times 10^{-6}r^3$
Central	621.4	-4.72	-3.55	-1.05
Blue edge	560.7	-4.07	-2.74	-1.20
Red edge	696.9	-5.42	-4.57	-0.81

**Note: Radius cf. position** (-7.9, -2.3)

$\mathbf{i'}$		$\times 10^{-2}r$	$\times 10^{-4}r^2$	$\times 10^{-6}r^3$
Central	753.3	-3.64	0.93	-1.04
Blue edge	683.1	-2.62	0.35	-0.93
Red edge	839.5	-5.29	2.14	-1.33

**Note: Radius cf. position** (4.8, 14.8)

$\mathbf{z'}$		$\times 10^{-2}r$	$\times 10^{-4}r^2$	$\times 10^{-6}r^3$
Central	879.4	-0.58	0.16	-0.22
Blue edge	841.8	-0.81	0.61	-0.66
Red edge	920.6	-0.52	-0.04	0.16

Where the radius is referred to an offset centre, its location is given in the  $(x, y)$  coordinates shown in Fig. 33.

## B Detector response curves

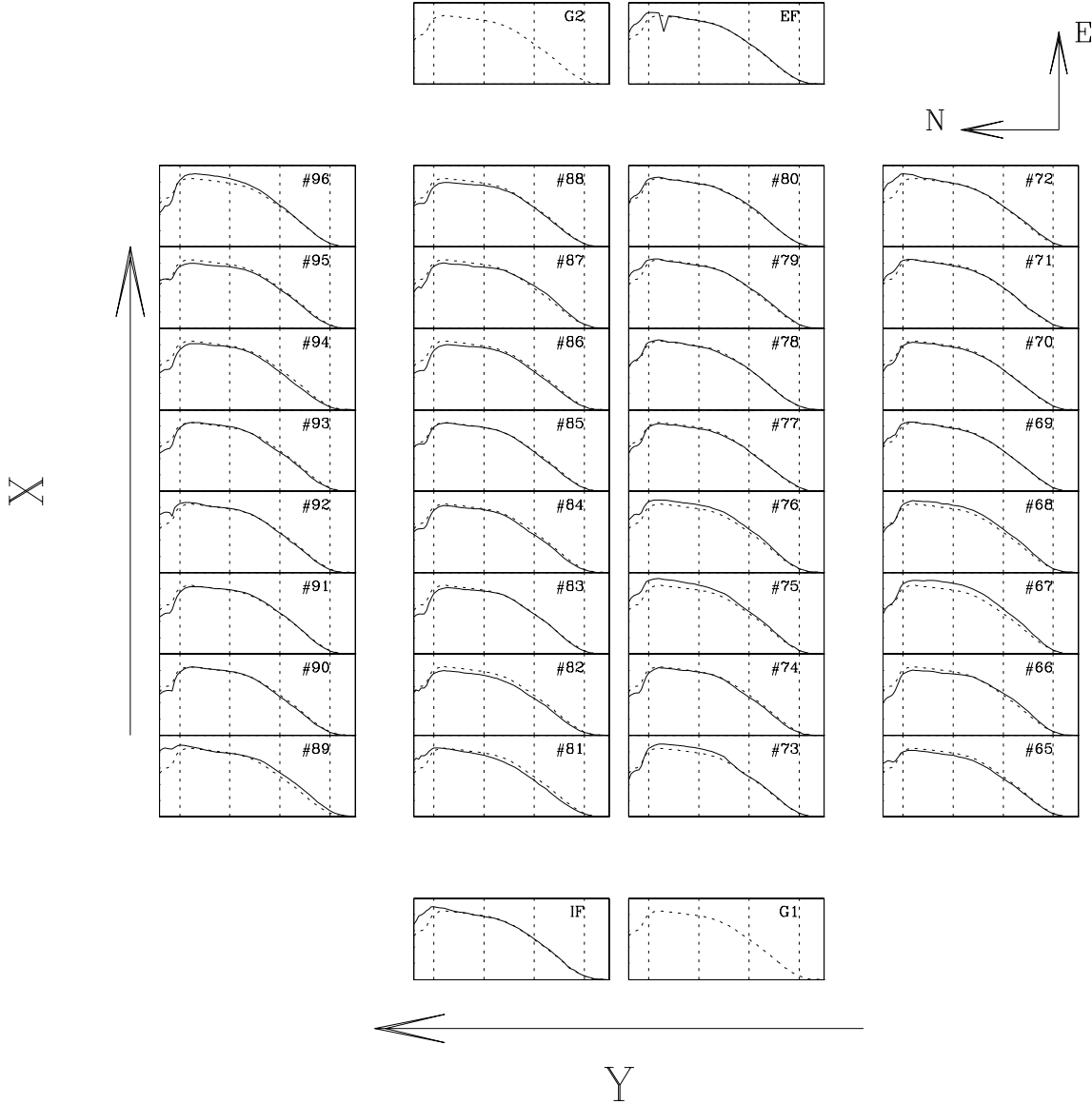


Figure 39: The QE curves for all CCDs in the mosaic, laid out as the mosaic itself (top view). The solid curve in each panel is the measured QE for that device; the dotted curve is the average for all 32 science CCDs. The wavelength range from 320 to 1100nm is plotted; dotted lines indicate 400, 600, 800 and 1000nm.  $X$  and  $Y$  are coordinates in the focal plane; for the default instrument rotator position angle of 0  $X$  points East and  $Y$  points North.

The CCDs labelled IF and EF are the intra- and extrafocal CCDs, for image analysis: these are mounted 2mm above and below the rest of the CCDs, respectively. G1 and G2 are guider CCDs.